Effects of substratum topography on bacterial adhesion
by Teresa Rush Scheuerman

A thesis submitted in partial fulfillment of the requirements for the degree of Master of Science in Chemical Engineering
Montana State University

Abstract:
It is known that bacteria tend to accumulate more on surfaces with high roughness than on smooth surfaces, but it is unknown whether these effects are due to heterogeneities in chemistry and/or topography. The effect of substratum topography on bacterial surface colonization has been studied here using a chemically homogeneous silicon coupon. “Grooves” ten microns deep and 10, 20, 30, and 40 microns wide were etched on the coupon perpendicular to the direction of flow. The local hydrodynamics of this topography were assessed using an in-house computer model.

The parallel plate flow reactor was inverted on the stage of a BioRad confocal scanning microscope to prevent bacterial settling. Flow of a bacterial suspension (10^8 cells/ml) was at a Re of 5.5. Images were collected to obtain rate and end point colonization data. Replicate experiments were run for each of three strains of bacteria: Pseudomonas aeruginosa, motile Pseudomonas fluorescens, and nonmotile Pseudomonas fluorescens. A higher velocity experiment was performed with the same cell concentration but at a Re of 16.6 to determine the effects of a higher velocity. A bead control was performed at a Re of 5.5 and the same particulate concentration to determine how the beads behaved relative to the bacteria. Finally, a conditioning film study was performed on a coupon which had been exposed to filtered chemostat effluent.

Using a colloidal deposition model, it was possible to compare the initial rates of attachment. The results showed that (1) P. aeruginosa had a higher rate of attachment than P. fluorescens mot + which had a higher rate of attachment than P. fluorescens mot-, (2) the rate of attachment was found to be independent of the groove size and was greatest on the downstream edges of the grooves, (3) the nonmotile organisms showed evidence of aggregation, (4) only the motile organisms were found in the bottoms of the grooves, (5) an increase in the fluid velocity resulted in a corresponding increase in the rate of attachment, (6) beads did not behave similarly to bacteria because they did not stick preferentially to the groove edges, and (7) no information could be gained on a possible protein layer because the coupon was contaminated with vacuum grease.

EFFECTS OF SUBSTRATUM TOPOGRAPHY ON BACTERIAL ADHESION

by

Teresa Rush Scheuerman

A thesis submitted in partial fulfillment
of the requirements for the degree

of

Master of Science

in

Chemical Engineering

MONTANA STATE UNIVERSITY-BOZEMAN
Bozeman, Montana
July, 1996

APPROVAL

of a thesis submitted by

Teresa Rush Scheuerman

This thesis has been read by each member of the thesis committee and has been found to be satisfactory regarding content, English usage, format, citations, bibliographic style, and consistency, and is ready for submission to the College of Graduate Studies.

John T. Sears (chair)	John T. Sears (Signature)	6-27-96 (Date)

Approved for the Department of Chemical Engineering

John T. Sears (Dept. Head)	John T. Sears (Signature)	6-27-96 (Date)

Approved for the College of Graduate Studies

Robert Brown (Graduate Dean)	(Signature)	7/8/96 (Date)

STATEMENT OF PERMISSION TO USE

In presenting this thesis in partial fulfillment of the requirements for a master's degree at Montana State University-Bozeman, I agree that the Library shall make it available to borrowers under rules of the Library.

If I have indicated my intention to copyright this thesis by including a copyright notice page, copying is allowable only for scholarly purposes, consistent with "fair use" as prescribed in the U.S. Copyright Law. Requests for permission for extended quotation from or reproduction of this thesis in whole or in parts may be granted only by the copyright holder.

Signature Teresa Rush Schuerman

Date 6-28-96

ACKNOWLEDGEMENTS

The help of the following people is greatly appreciated: Anne Camper, who was the project leader and a dear friend; Marty Hamilton, who helped discover a new way to analyze the data and helped with the statistical analysis and interpretation; Brian Schneider, who did most of the statistical analysis; Tim Minton, who obtained the coupons; Gary Harkin, who wrote the MARK software; Ernie Visser, who did the hydrodynamic modelling; Doug Cairns and Robert Hunter, who gave me ideas about the hydrodynamic effects; Pat Schamberger, who did all of the surface analysis; Brian Goldstein, Brian LaMettery, and Jesse Block, who all saved my files at one time or another from computer failure and worked out many software and hardware glitches; John Neuman, Ace Baty, Shannon Bakich, and Paul Stoodley, who helped me with different laboratory procedures and in obtaining equipment; Peg Dirckx and Jamie Pennington for their help with slides and graphics.

I would also like to express my thanks to my family for their support and to my husband, Marty, whose nearly unlimited love and patience helped keep us together even though we were living 1500 miles apart for nearly two years.

TABLE OF CONTENTS

LIST OF TABLES

Table Page

LIST OF FIGURES

ABSTRACT

It is known that bacteria tend to accumulate more on surfaces with high roughness than on smooth surfaces, but it is unknown whether these effects are due to heterogeneities in chemistry and/or topography. The effect of substratum topography on bacterial surface colonization has been studied here using a chemically homogeneous silicon coupon. "Grooves" ten microns deep and 10, 20, 30, and 40 microns wide were etched on the coupon perpendicular to the direction of flow. The local hydrodynamics of this topography were assessed using an in-house computer model.

The parallel plate flow reactor was inverted on the stage of a BioRad confocal scanning microscope to prevent bacterial settling. Flow of a bacterial suspension (10^8 cells/ml) was at a Re of 5.5. Images were collected to obtain rate and end point colonization data. Replicate experiments were run for each of three strains of bacteria: *Pseudomonas aeruginosa*, motile *Pseudomonas fluorescens*, and nonmotile *Pseudomonas fluorescens*. A higher velocity experiment was performed with the same cell concentration but at a Re of 16.6 to determine the effects of a higher velocity. A bead control was performed at a Re of 5.5 and the same particulate concentration to determine how the beads behaved relative to the bacteria. Finally, a conditioning film study was performed on a coupon which had been exposed to filtered chemostat effluent.

Using a colloidal deposition model, it was possible to compare the initial rates of attachment. The results showed that (1) *P. aeruginosa* had a higher rate of attachment than *P. fluorescens* mot + which had a higher rate of attachment than *P. fluorescens* mot-, (2) the rate of attachment was found to be independent of the groove size and was greatest on the downstream edges of the grooves, (3) the nonmotile organisms showed evidence of aggregation, (4) only the motile organisms were found in the bottoms of the grooves, (5) an increase in the fluid velocity resulted in a corresponding increase in the rate of attachment, (6) beads did not behave similarly to bacteria because they did not stick preferentially to the groove edges, and (7) no information could be gained on a possible protein layer because the coupon was contaminated with vacuum grease.

INTRODUCTION

About Biofilms

A biofilm is formed in a four-step process consisting of (1) transport of the cell to the substratum, (2) initial, reversible adhesion of the cell to the substratum, (3) irreversible attachment of the cell, and (4) colonization of the substratum. The process occurring during early colonization at the solid-liquid interface can be summarized as follows (Mueller, et al. 1992):

(1) Conditioning of the substratum by organic molecules
(2) Transport of cells from the bulk water to the solid-liquid interface
(3) Adsorption of cells on the substratum
(4) Transformation of reversibly adsorbed cells to irreversibly adsorbed cells
(5) Desorption of reversibly adsorbed cells from the substratum into the bulk water
(6) Growth of irreversibly adsorbed cells
(7) Erosion of cells from adsorbed colonies into the bulk water

Biofilms can also consist of macroorganisms, corrosion by-products, particulates, etc.

Biofilms can be a benefit to society, for example, they are used for immobilization of microorganisms for wastewater treatment and other enzymatic conversions, metal leaching in biohydrometallurgy, and removal of dissolved and particulate contaminants in natural streams and in waste water treatment plants. They are also used in some common fermentation precesses, e.g., the "quick" vinegar process (Characklis and Marshall 1990), and they are used regularly in the pharmaceutical industry.

Biofilms can also be detrimental, for example the fouling of heat exchangers (increasing the heat transfer resistance), thrombus formation in vascular prostheses, and plaque formation on teeth. They can induce corrosion, increase frictional resistance in pipes, increase the drag on a ship, and influence the hygienic safety of municipal water supply and processed food.

The remainder of this paper is concerned with the events occurring during the initial formation of biofilms. The initial formation consists of steps one through five. This work is specifically about steps 2, 3, and 4. The study of initial attachment of bacteria to surfaces is very important in work on porous media, medical implants, and in the oral cavity.

Previous Work

Systems and Related Transport Mechanisms

Many systems have been used to study the adhesion of cells to a given substratum. These systems can be divided into two different categories - static and flow.

Static. A static system is generally described as "no-flow." It is a closed system in which the fluid either does not move relative to the substratum, or there is random and poorly controlled fluid movement. Static systems are preferred in experimentation when the natural situation is stagnant or when the adhesion studied must be reversible. Some examples are the study of the effects of cell motility (Piette and Idziak 1991; Frymier

1995) and the effect of cell surface hydrophobicity on cellular adhesion (Vanhaecke et al. 990)

Flow. Flow cell systems allow proper control of the hydrodynamic conditions in terms of shear rate, flow velocity, and Reynolds number, which determine the mechanism of mass transport. Flow cells are preferred to a static system if flow occurs in the natural situation. There have been several kinds of flow chambers used in the study of bacterial adhesion. The radial flow chamber, which is comprised of two parallel circular plates with the flow inlet in the center, was used to study the effects of shear stress on attachment (Duddridge et al.1982).

The parallel plate flow cell has been the flow cell of choice for recent studies (Mueller et al. 1992; Camper et al. 1994; Meinders et al. 1992; Sjollema et al. 1989-2; Sjollema and Busscher 1990; Sjollema et al. 1990-2;Van der Mei et al. 1994; Pedersen 1990; Mueller et al. 1992; Bowen and Epstein 1979; Busscher, Doornbush and Van der Mei 1992) because it allows observation of the deposition process *in situ*. Passage of the substratum through an air-water interface for rinsing, fixation, or staining procedures for the attached bacteria can be avoided by substituting the suspension with fixative and rinsing solutions. This is described since an air-water interface exerts a force parallel to the substratum surface of approximately 10^{-2} dynes (Busscher et al. 1990). Such a force may cause spatial rearrangement or detachment of adhering cells and may introduce artifacts in the enumeration of attached cells. The parallel plate flow cell has also been used to study cell-cell interactions (Cowen and Busscher 1993).

The transport of bacteria to the surface is controlled by a combination of diffusion and convection. For a parallel plate flow chamber operating in laminar flow, convective transport is parallel to the substratum surfaces and cell transport to the surface is by diffusion, sedimentation, and sometimes attractive interaction forces (hydrophobicity, charge). Collisions between flowing particles to give them a velocity component towards the surface, sedimentation, and attractive interaction forces are required for a bacterium suspended in flowing fluid to cross the boundary and diffusion boundary layers and reach the surface (Van der Mei, Meinders, and Busscher 1994). Diffusion is a critical component of cell-surface interaction. For example, it can take minutes for an average micro-organism to reach the substratum by diffusion only. In the parallel plate reactor diffusion is obviously the rate determining factor for deposition as it is much slower than convection. Therefore, a micro-organism reaching a substratum surface by diffusion only is rather limited. Cell motility is also important and can act to increase the effective diffusivity of the cells to the surface by up to four orders of magnitude (Mueller 1990).

The relative importance of convection and diffusion in these systems is further defined by the Peclet number, which determines the ratio between motion due to convection and diffusional motion:

$$Pe = \frac{VL}{D} \qquad (1)$$

where V = the mean flow velocity; L = a characteristic length, for instance the separation distance of the plates in a parallel plate flow-cell; and D = diffusion coefficient. High

Peclet numbers imply thin boundary layers and vice versa. The mass transfer coefficient, k, is often expressed in a dimensionless Sherwood number:

$$Sh = \frac{kL}{D} = \frac{L}{\delta} \qquad (2)$$

where δ = the diffusion boundary layer which generally ranges between 0.1 μm and 100 μm although exact numerical relations are difficult to compute (Sjollema et al. 1989-1). The boundary layer for diffusion is considerably thinner than the boundary layer for flow (Van der Mei, Meinders, and Busscher 1994). If the diffusion boundary layer is large, the influence of a potential barrier due to repulsive electrostatic interaction upon the deposition process is decreased. However, if the boundary layer is extremely thin, Van der Waals attraction will be the rate-determining step (Sjollema et al. 1989-1). For bacterial transport, this means that if the boundary layer is thick, then no matter how great the Van der Waals attraction, the cells still have to diffuse through the thick boundary layer. On the other hand, if the boundary layer is thin, then the Van der Waals attractive forces will be the main mechanism of the cells reaching the surface because they are already close to the substratum.

Colloidal Particles

Colloidal particles are useful in studying the kinetics of deposition (Sjollema and Busscher 1990) as well as the effects of ionic strength and flow rate (Meinders et al. 1992). Particles make it possible to study adhesion in the absence of growth because the particles do not react with the substratum or the aqueous phase. Particles have also been

used to study the effect of the electrical double-layer interactions on the deposition rate (Bowen and Epstein 1979). These colloidal particles are nice to study because the transport ideally is identical to nonmotile cells.

Kinetics

The kinetics of cellular and particulate adhesion have been extensively studied (Sjollema et al. 1989-2; Meinders et al. 1992; Mozes and Rouxhet 1992; Bowen and Epstein 1979; Sjollema and Busscher 1990). The kinetics can be generalized as shown in Figure (1) using the function of particle deposition (Meinders et al. 1991)

$$number\ of\ particles\ adhering = \frac{J}{B}(1-e^{-Bt}) \qquad \textbf{(3)}$$

where J is the slope of the function at time t equals zero is shown. The plateau occurs at a number of particles = J/B. This function can be used to describe the initial attachment of bacteria where the plateau is in the absence of cell growth. Therefore, the adhesion of a bacterial strain under defined conditions can be expressed as a combination of the constants J and B.

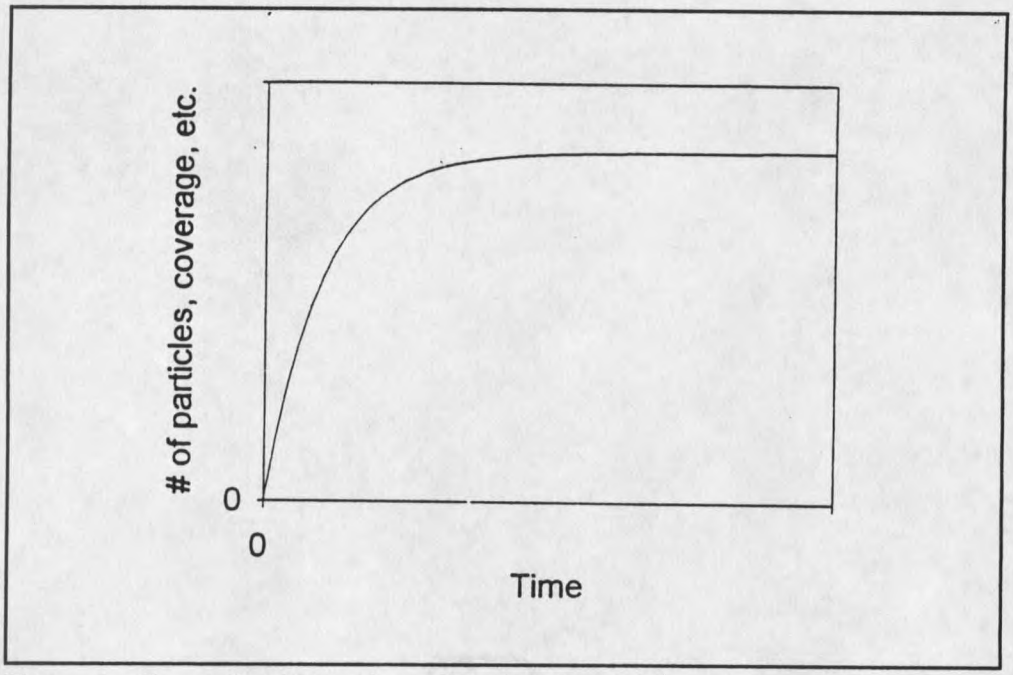

Figure 1. Generalized Function of Particle Deposition.

Physico-Chemical Effects

Interactions by which microorganisms can adhere to a solid surface are all manifestations of three basic physico-chemical forces: Liftshitz-Van der Waals forces, electrostatic forces, and hydrogen bonding (Busscher et al. 1992-2). These interactions can be stated as a function of distance between the cell and substratum (Busscher et al. 1992-2):

> >50 nm only Liftshitz-Van der Waals forces operate. At this distance nonspecific macroscopic cell surface properties play the most dominate role.
>
> Between 10 and 20 nm additional electrostatic repulsion becomes active, resulting in a reversible adhesion.

> At <1.5nm specific interaction can take place, provided the organism is capable of sending out adhesion probes and hydrophobic groups are available to dehydrate the surface, allowing direct contact. This capacity is bacterial strain-dependent.

There exist two theories regarding the attachment of cells to a substratum, DLVO and thermodynamics. The DLVO theory proposes that adhesion is mediated by attractive Lifshitz-Van der Waals forces as well as attractive or repulsive electrostatic forces. The thermodynamic theory is based upon the free energy of adhesion by deriving the surface free energies of the cell and substratum surfaces. These two theories assume that the transport of the cells to the substratum is not limiting.

DLVO Theory. In the Derjaguin-Landau and Verwey Overbeek (DLVO) theory, adhesion is thought to be mediated by attractive Lifshitz-Van der Waals forces and attractive or repulsive electrostatic forces. The DLVO theory is based upon on the "macroscopic" cell surface properties with no regard to cell or substratum surface heterogeneity - chemical or structural. Therefore, the DLVO theory is only useful in describing the approach of a cell in reversible adhesion. Following reversible adhesion, specific groups on the cell (and possibly the substratum) can reorient themselves and strong, irreversible adhesion occurs. In order to achieve close placement of stereo-chemical groups, interfacial water has to be removed from between the cell and the substratum surface. The removal of interfacial water may be accomplished with two hydrophobic surfaces coming in contact, removing the water. Thus, the term "cell surface hydrophobicity" came about (Busscher et al. 1992-2). Cell surface hydrophobicity will be discussed later.

As two surfaces approach each other, the DLVO theory allows the computation of the interaction potential energy, or tendency to associate. The overlap of diffuse double layers of charge is responsible for electrostatic interactions at a separation distance of several tens of nm (Mozes and Rouxhet 1992). If the two surfaces are of the same charge, a potential barrier decreases the probability that the two surfaces will form a firm bond. Conversely, if the two surfaces are oppositely charged, the probability of forming a firm bond increases. Because bacteria are generally negatively charged in their natural medium, attraction occurs only with surfaces of positive charge. Solid materials are also generally negatively charged (Mozes and Rouxhet 1992) - creating an electrostatic repulsion with microbial cells. "The DLVO theory is not sufficient for explaining deposition phenomena" because negatively charged particles have deposited on negatively charged subtratum, overcoming the electrostatic repulsion (Sjollema and Busscher 1990).

Thermodynamics. Another approach (besides the DLVO theory) is based on thermodynamics. In a thermodynamic approach, contact angle data (described later in the cell surface hydrophobicity section) are used to derive the surface free energies of the solid and bacteria which then are used to calculate the free energy of adhesion. Free energy of adhesion is computed by regarding the transformation of two solid-liquid interfaces to a single solid-solid interface. If the free energy of adhesion is negative, then adhesion is favored thermodynamically. The surface free energy of the liquid phase is usually determined tensiometrically. Interfacial free energies are computed from contact

angles of liquids and do not incorporate the contribution of electrostatic interactions between the two solids (Mozes and Rouxhet 1992). A surface with high surface energy is hydrophilic (Sorongon et al. 1991).

Cell Surface Hydrophobicity. Cell surface hydrophobicity is frequently measured by water contact angle measurements, MATH (microbial adhesion to hydrocarbons test), and interaction chromatography. To determine the contact angle for the bacteria, a bacterial lawn is produced on agar plates or on membrane filters to achieve a surface large enough to determine contact angles. Because the measurements are performed on a large number of cells, the results are representative of the entire population and do not account for variations within the population. Contact angle measurements are reported as the angle formed when an air bubble or a drop of water approaches a bacterial lawn as well as the spread direction of a drop of water placed at an interface of a bacterial lawn and a nonbiological medium (either hydrophobic or hydrophilic). MATH and HIC (hydrophobic interaction chromatography) methods measure the interaction between a hydrophobic solid and dispersed cells suspended in water. These results distinguish between hydrophobic and hydrophillic cells in a population (Bar-Or 1990). Because cell surface hydrophobicity is often measured on whole cell suspension, the results reflect an average over the population and do not account for variability within the population or on individual cell surfaces.

Depending upon which method is used to determine the cell surface hydrophobicity, major differences in the ralative hydrophobicity of the organism(s) are

found (Vanhaecke et al. 1990, Bar-Or 1990). Therefore, several methods have been used in conjunction in recent work.

Using cell surface hydrophobicity measurements to describe adhesion does not work well. For example, it has been shown that the adhesion of *Streptococcus sanguis* 12 was less on a hydrophobic surface (FEP) than on a hydrophillic surface (glass) (Busscher et al. 1990). On the other hand, it has also been shown that there was no difference in adhesion between a hydrophilic steel surface and hydrophobic PVC (Pedersen 1990). Another study showed that bacterial adhesion to glass did not correlate with any measure of cell surface hydrophobicity (Sorongon et al. 1991).

Hydrophobicity has also been found to vary with cell growth conditions and environmental conditions. For example, the hydrophobicity in some bacteria increased with increasing dilution rate of the growth medium. The temperature can affect the cell hydrophobicity for example, a change of 7°C in growth medium will cause *Serratia marcescens* to lose its hydrophobicity as measured by MATH (Van der Mei et al. 1992). It has also been shown that a given bacterium can interact either hydrophobically or electrostatically or both depending on the media, substratum, and cell (Bar-Or 1990). The relative importance of hydrophobicity in attachment is likely low, as (1) there is no clear trend in whether cell attachment is based upon hydrophobicity measurements and (2) the cell surface hydrophobicity is not necessarily constant for an organism.

Electrostatic Interactions. Work with colloidal particles has also shown that surface interaction forces greatly retard the deposition rate when the substratum and the

particles are similarly charged. Whenever a stable suspension of relatively homogeneous particles is involved, surface interaction forces greatly restrict the total number of particles which can be accommodated on the channel wall. Thus, even monolayer converage is never approached. (Bowen and Epstein 1979).

One way of measuring this charge interaction between bacteria or particles and a substratum is called the zeta potential. To determine the zeta potential, bacteria are suspended between two charged plates immersed in the medium. The generated electric field causes the charged bacterium to move. The electric field is manipulated until the bacterium is stationary, and the zeta potential is the final potential between the two charged plates. It has been shown that there is a possibility of several zeta potentials in the same organism (Cowan et al. 1992-2). It is also well-known that bacteria change their surface composition in response to the environment (Cowan et al. 1992-1).

Integration of Physico-Chemical Parameters. These physico-chemical approaches are often criticized for not accounting for the microscopic stereochemical complementary molecular interactions between the surfaces. Therefore, Busscher and his colleagues related elemental composition by XPS, surface free energy by contact angles, and isoelectric point for oral streptococci even though they were analyzed at different states of hydration (Busscher et al. 1989). Oxygen was responsible for high surface free energies and low isoelectric points. High nitrogen content from surface proteins, on the other hand, resulted in low surface free energies and high isoelectric points.

Cell Structure Effects

It has been theorized that cell appendages may bridge the distance between the cell and surface because of their small radii or more hydrophobic character than the remainder of the cell (Mozes and Rouxhet 1992; Sjollema et al. 1990-2). However, Piette and Idziak demonstrated that the flagellum is no different from the cell surface in hydrophobicity or surface charge but the small radius makes it more prone to adhesion than the cell body (Piette and Idziak 1991). It has also been stated that cell surface appendages or excretion of adhesives assist or impede adhesion in excess of strictly thermodynamic considerations. (Busscher et al. 1989)

Piette and Idziak have shown that flagellated cells attached in greater numbers than deflagellated cells (*Pseudomonas fluorescens*) (Piette and Idziak 1991). This effect has been attributed entirely to the ability of motile organisms to reach the surface more often. In their studies, motile cells attached to a surface initially by their polar flagella and then rotated. The cell then detached and swam away or stopped rotating and became firmly attached. However, flagella do not appear to be necessary for adhesion because even nonmotile cells have been shown to attach (Piette and Idziak 1991).

Extensive work has been done in the marine community on the initial attachment of barnacle larvae. Even though the larvae are much larger than bacteria, they do tend to behave similarly. Mucous threads secreted by the aboral part of cypris larvae are used to overcome impedance through two phases of settlement. In the first phase, the threads increase the efficiency of encounter with the substratum. In the second phase, the

threads allow instantaneous attachment to the substratum - therefore, the larvae does not need a short time of locally calm flow conditions to attach (Abelson et al. 1994).

Mechanical Effects

Conditioning Film. A conditioning film is a layer, generally proteinaceous, that adsorbs to a surface. It may contain organic molecules, metallic hydroxides, hydrated oxides, and very fine clay mineral materials. There are two basic forms of a conditioning film (1) a film adsorbed to a substratum arising from the solution, and (2) a film laid down on a substratum by the cell itself. Not much work has been done on the films formed by the cells, so the remainder of this section deals with the former.

These conditioning films are proported to have a dramatic effect on the initial adhesion of bacteria. It is hypothesized that the conditioning film changes the surface that the bacteria "see." For example, the conditioning film can change the hydrophobicity of the substratum. However, it has been shown that some substratum characteristics are evident even through a thick conditioning film (Busscher et al. 1992-2). Adsorption of macromolecules such as proteins and polysaccharides compose the conditioning film on the substratum surface. The onset of this adsorbed layer (conditioning film) is extremely rapid compared with the arrival of bacteria. These adsorbed layers may influence bacterial adhesion by: modifying the physico-chemical properties of the substratum, acting as a concentrated nutrient source, suppressing the release of toxic metal ions from the substratum, detoxifying dissolved inhibitory

substances, acting as a source of required metal trace elements, and acting as a triggerable sloughing mechanism (Chamberlain 1992).

Studies have been performed on the adsorption of fibrinogen and albumin from human blood plasma onto chemically functionalized substrates (Wojciechowski and Brash 1993). In single protein systems neither albumin nor fibrinogen adsorption was strongly correlated with advancing water contact angle although a slight increase in the initial rate of adsorption was found with increasing contact angle. Fibrinogen adsorption was correlated with surface chemistry in that sulfur coincided with increased adsorption and nitrogen with decreased adsorption. Andrade's group has studied the adsorption of simple proteins to simple surfaces and have developed a multivariate analysis technique to determine the kinds of surfaces that will resist protein adsorption. They have shown that PEO (polyethylene oxide) surfaces greatly decrease protein adsorption (Andrade et al. 1992).

In medical applications where the desired response is the attachment of tissue to a biomedical implant, it has been shown that cells require adhesion proteins to adhere and spread. Spreading of tissue cells was low on low surface free energy substrata and high on high surface free energy substrata after preconditioning with serum proteins. However, cellularly produced proteins (possibly adhesion proteins) seem to be able to displace adsorbed serum proteins from biomaterial surfaces implying that cells have a higher affinity for self-produced proteins than for noncellular proteins (Schakenraad et al. 1992). If this is the case, then the implication is that the bacteria will displace the

attachment of body tissue, causing an infection. Therefore, it is of great interest to study the adhesion of both types of proteins - serum and bacterial.

Conditioning films in the oral cavity have been relatively well studied (Quirynen et al. 1991; Busscher, Doornbush, and Van der Mei 1992; Busscher et al. 1992-2). The oral cavity rapidly adsorbs salivary proteins, changing the surface free energy of the enamel as well as of the bacteria (Quirynen et al. 1991). Bacterial retention was much higher on hydrophilic substrata than on hydrophobic substrata and dependent on rinse flow rates but not temperature; therefore, the salivary film must be different on hydrophobic than on hydrophilic substrata (Busscher et al. 1992-2).

Saliva-coated hydroxyapatite beads showed that a general effect of a protein coating is to reduce microbial adhesion (Busscher et al. 1992-2). It is hypothesized that the adsorbed mucin layer was modified by the substratum hydrophobicity, revealing hidden high affinity binding sites. The adhesion of *Streptococcus* to glass decreased after saliva coated the glass (Busscher, Doornbush, and Van der Mei 1992). More work with Streptococci showed that adhesion decreased after precoating with proteins and that surface free energy effects were transferred through adsorbed protein films (Busscher et al. 1989). It is hypothesized that the salivary conditioning film makes adhesion less efficient and more time consuming because stereochemical groups in the saliva and on the cell surfaces may have to rearrange before an effective interaction can occur. The structure and composition of the salivary conditioning film may be more important to adhered cell retention than the cell-surface properties (Busscher, Doornbush, and Van der Mei 1992).

Surface Roughness. Effects of substratum topography have been studied for more than fifty years (Gregg 1948; Pomerat and Weiss 1946). It has been hypothesized that bacteria stick to rougher surfaces because of three reasons: (1) a higher surface area available for attachment, (2) protection from shear forces, and (3) chemical changes that are generally involved.

Most of the early work was performed in the marine environment. Barnacles of the species *Balanus eburneus* were found to orient themselves with their long axes parallel to the grooves in the substratum. The substratums used were phonograph records! (Gregg 1948) It has also been shown that the selectivity of free-swiming cyprid larvae to the substratum is related to the heterogeneity of the substratum. Rough surfaces are favorable for settlement of barnacle cyprids (Hudon et al. 1983).

In the Gulf, cypris larvae settled nearly exclusively (93%) in natural crevices (>10 cm) rather than on adjacent horizontal surfaces. This effect was opposite on the Atlantic coast. On a small scale (<1.5 cm), presence of other life had larger effect than heterogeneity. Also, settlement was significantly greater on grooved surfaces than on smooth surfaces (Chabot and Bourget 1988).

It seems to be a common theme that cyprids "choose" where they settle. When they are offered a 'choice' between a large area of plane surface and a number of special sites, settlement was much heavier in the grooves than on plane surfaces. This effect decreased with increased settlement. It was theorized that settlement in a small hollow is advantageous to the cyprid larvae, ensuring both an inital key for the permanent adhesion

as well as a degree of protection. If the cyprids are on a smooth surface, whole sheets may be removed as opposed to cyprids on rough surfaces. Settling on a rough surface helps to ensure their survival. (Crisp and Barnes 1954).

Yet another study has shown that the typical settlement site had an uneven surface, due to the visible presence of mussel growth ridges, algal cells, or plastic striation. On natural substrate, half the barnacle cyprid larvae were found in grooves (note: grooves made up less than half of the surface), usually parallel to one another. The larvae generally settled in the widest part of the groove (Hudon et al. 1983). Here again, the larvae "choose" to adhere where there are grooves, preferentially in the bottoms of the grooves. However, the increase in total area due to imposed grooves on the surface had no significant effect on settlement (Chabot and Bourget 1988).

Grooves have an influence on bacterial attachment because there is a formation of vortexes in a valley which can favor adhesion on the bottom of these valleys. As valley width increases, the probability of vortex formation decreases and it is theorized that a more uniform colonization will occur (Schmidt 1995).

Work with bacterial suspensions has shown that a rough surface (matt steel) had 1.44 times more microorganisms attached than a smooth surface (electro-polished steel) (Pedersen 1990). Adhesion rate constants of *Pseudomonas aeruginosa* to electopolished 316-L plates were about 100 times lower than those to 120-grit surfaces (Vanhaecke 1990). Adhesion of yeast cells on stainless steel was at a minimum for medium surface roughness (R_a=1-6μm as measured using a Rayleigh perturbation relationship). (Schmidt 1992)

Oral plaque growth patterns have been found to correlate closely with irregularities in the tooth surface. Also, the rate of bacterial colonization of intra-oral hard surfaces was positively correlated with surface roughness. It was hypothesized that there was a preferential change from weak and reversible binding to irreversible binding in the niches of surface irregularities where the microorganisms were protected from shear. The effect of surface roughness on plaque formation was more prominent than the influence of surface free energy. Roughness not only increased plaque area but also height (Quirynen et al. 1991).

Substratum microroughness may affect bacterial adhesion in many different ways. The chemistry could be different causing the interaction between a particle and the substratum to be strongly dependent upon the nature of the local areas coming into contact (Bowen and Epstein 1979). Henk Busscher and his collegues at the Laboratory for Materia Technic in The Netherlands have hypothesized that no matter how strong the adhesion forces, motion of adhering cells over a surface remains possible on perfectly smooth and homogeneous substrata and that only surface roughness or chemical heterogeneity can induce real immobilization (Busscher et al. 1990; Sjollema et al. 1990-2). Surface microroughness may help attachment of cells in that (1) there is more surface area available for cell-substratum contact and (2) cells located inside pores are sheltered from shear forces; therefore their removal rate is reduced and retention of a larger amount of cells is assured (Mozes and Rouxhet 1992). Detachment of bacteria due to shear forces from the flow was reduced on rougher surfaces because of shielding from shear as well as from more surface area available for attachment. (Pedersen 1990)

Work on stainless steel has shown that bacteria were associated with the grain boundaries of stainless steel (Gillis 1993). However, the grain boundaries have not only a change in topography, but also a change in chemistry. Grain boundaries have precipitation of $(Fe, Cr)_{23}C_6$ particles with an accompanying depletion of chromium from the regions adjacent to the boundary (Lumsden and Stocker 1981). Because changes in topography are coexistent with changes in chemistry, the two effects must be separated.

The potential interaction of topography and chemistry may also be seen in the study of weld corrosion. In the study of microbially influenced corrosion, Roughness near the weld surface was proported to promote colonization and subsequent corrosion (Walsh et al. 1993). Also, microbes aggregated in the depressions between dendrite arms in the weld structure. The study also showed that microbes tended to be localized at inclusions, the average length of which was 0.028-0.0019mm. The authors state that large inclusions in stainless steel have a greater gross sulfur content, a greater probability of being contacted by microbes attaching to the surface, and can support a higher concentration of dissolving species in the solution for a longer period of time. However this study could not characterize local changes in terms of the substratum topography vs chemistry.

Hydrodynamics. Changes in the flow conditions allow researchers to determine the effects of hydrodynamics. Earlier, it was noted that cells tend to be associated with the weld structure in stainless steel. The same work noted that there was stagnant water at the weld crown and roots, particularly where undercut, suck-back, or excessive

reinforcement exits (Walsh et al. 1993). It has been noticed that cells deposit in milling crevices because they are protected from shear arising from flow. In addition, cells frequently are observed in "streamers" following milling marks at right angles to the flow (Duddridge et al. 1982). Could it be that there is an effect of hydrodynamics on adhesion?

The effects of shear stress have also been studied. Duddridge's group (Duddridge et al. 1982) studied a wide range of shear stresses and noticed that the cells transported to the surface attached reversibly and were washed off again at rates increasing with the surface shear stress. There was a critical surface shear stress of 6-8 N/m^2 when the extent of attachment dropped off sharply. As the surface shear stress increased, the rate of transport of bacteria to the substratum was expected to increase as well, but did not increase the rate of attachment (Duddridge et al. 1982). Because the work was done in a radial flow chamber, it would have been impossible to keep the cell concentration the same everywhere in the flow chamber, so it could have been possible to increase the rate of transport to the surface while having a decrease in the rate of attachment. Busscher and his collegues noted that when adhering cells are subjected to an air-water interface, a large number of them detach due to the shear force, causing errors in cell enumeration when the surfaces are "slightly rinsed" (Busscher et al. 1990).

Again, study of marine propagules has included the study of hydrodynamics. No settlement of marine propagules was observed in decelerating flow, but there was a high ability of the animal to encounter and attach to substrata in accelerating flows (Abelson et al. 1994).

It appears that the effects of hydrodynamics far outweigh the physico-chemical effects on bacterial adhesion. The physico-chemical effects are extremely short-distance effects. If the cells are in that short distance from the substratum, then the physico-chemical effects could make a difference on the rates of adhesion. However, the cells have to be transported to that very short distance from the substratum for those effects to make much difference. It seems that cellular adhesion is limited by transport, thus the hydrodynamics of the situation.

Current State of the Art

Because it is plainly evident that the effects noted above (physico-chemical, conditioning film, mechanical) do not exist in isolation, the current state of the art in studying bacterial adhesion includes combining physico-chemical effects and mechanical effects. A few examples follow. Several researchers have combined the effects of substratum roughness and hydrophobicity (Mueller et al. 1992; Pedersen 1990; Vanhaecke 1990). The results of this work show that the adsorption rate was positively correlated with surface free energy, the surface roughness of the substratum, and the hydrophobicity of the cells. Also, the probability of desorption decreased with increasing surface free energy and substratum surface roughness (Mueller et al. 1992). Quirynen et al have combined the effects of substratum roughness, surface free energy, and conditioning films and found that the plaque growth patterns of oral bacteria closely followed the tooth irregularities and the rate of bacterial colonization was positively correlated with the surface roughness and the surface free energy. They also found that

the oral cavity rapidly adsorbs salivary porteins, changing the surface free energy of the enamel and of the bacteria (Quirynen et al. 1991). Another example is the combination of physico-chemical effects and a conditioning film where it was found that the surface free energy effects are transferred through adsorbed protein films (Busscher et al. 1989).

Current Work

Once the mechanisms behind adhesion of bacteria to substrata are known, it will be possible to model systems and include the initial events of bacterial adhesion. It is desired to determine whether the position of the bacteria are associated with surface topography or with surface chemisty, or both. To accomplish this goal, it is necessary to quantify topographic features while holding substratum chemistry constant. The motivation of this work is to study the effects of hydrodynamics as mediated by topography on bacterial adhesion. Modelling will not be the only benefit. Once the effects of topography are known, the design of equipment to be used in industy can be changed to take the effect into account. For example, the joints in water piping are already being redesigned to minimize the risk of microbial contamination (Artiss 1982).

MATERIALS AND METHODS

The objective of this research was to determine the effects of local hydrodynamics on bacterial adhesion. The adhesion of *Pseudomonas aeruginosa*, *Pseudomonas fluorescens* mot +, *Pseudomonas fluorescens* mot -, and spherical beads were examined. Also, the composition of any conditioning film was determined. To accomplish a change in local hydrodynamics, the substratum topography was changed while keeping the chemistry homogeneous.

Coupon

A surface was needed that would remain chemically homogeneous even after the topography was changed. Silicon was the surface of choice. The Center's Microscale Microbial Process model (MMP model) was used to determine the topography to be imposed, which was initially selected to be rectangular grooves perpendicular to the intended flow of suspended bacteria. MMP combines fluid dynamics, substrate transport and biofilm growth on walls (Chen et al. 1994, Cunningham et al. 1995). Navier-Stokes equations are used for solving for velocity which then is used in solving species balance equations for dissolved constituents. For the purpose of this research only the fluid dynamics portion was used. A Reynold's number (characteristic length = the depth between two parallel walls of the parallel plate reactor as the depth/width ratio was

small) of 6 was used in the modelling to determine the groove widths that would be used.

Figure 2 shows the effect of a groove that is 10 μm deep and 10μm wide as determined by the MMP model. It can be seen that there is a slight dip in the stream functions. Figure 3 shows the effect of a such groove that is 10 μm deep and 40 μm wide, where there is a dramatic effect on the local hydrodynamics. There are eddies in the bottom corners and there is a region of non-zero stream function even at the bottom of the groove. It was decided that grooves 10μm deep and varying in width from 10-40μm would be used to study the effects of local hydrodynamics on bacterial adhesion. Two sets of the four grooves were chosen for statistical purposes. One set increased in size from 10 - 40μm (first half) and the other set decreased from 40 - 10μm (second half). This pattern has the two widest grooves in the center of the coupon and reduces the effect of any linearity in adhesion across the coupon. Also, it prevents the same size groove from influencing the downstream attachment. Figure 4 shows a schematic and naming convention for the samples of the chosen coupon.

These grooves were created on the surface of the silicon by chemical etching (See Appendix A). In the following experiments, the grooves are consecutively numbered from right to left with the 10μm groove on the right as number 1 and the 10μm groove on the left being number 8. Groove size and morphology was verified on a coupon that had fractured (see Appendix A) by using a Scanning Electron Microscope aimed at the cross-section and top of the grooves.

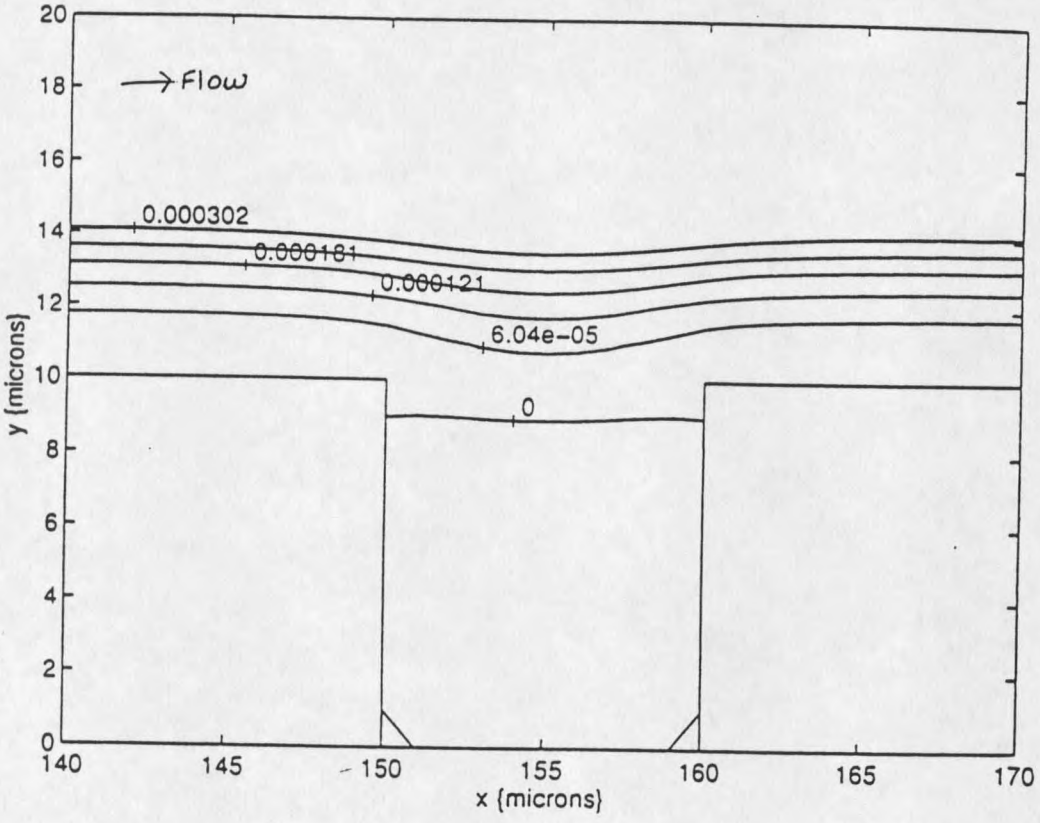

Figure 2. MMP Model Showing Stream Functions around the Cross-section of a Groove 10μm Wide and 10μm Deep. Re=6.

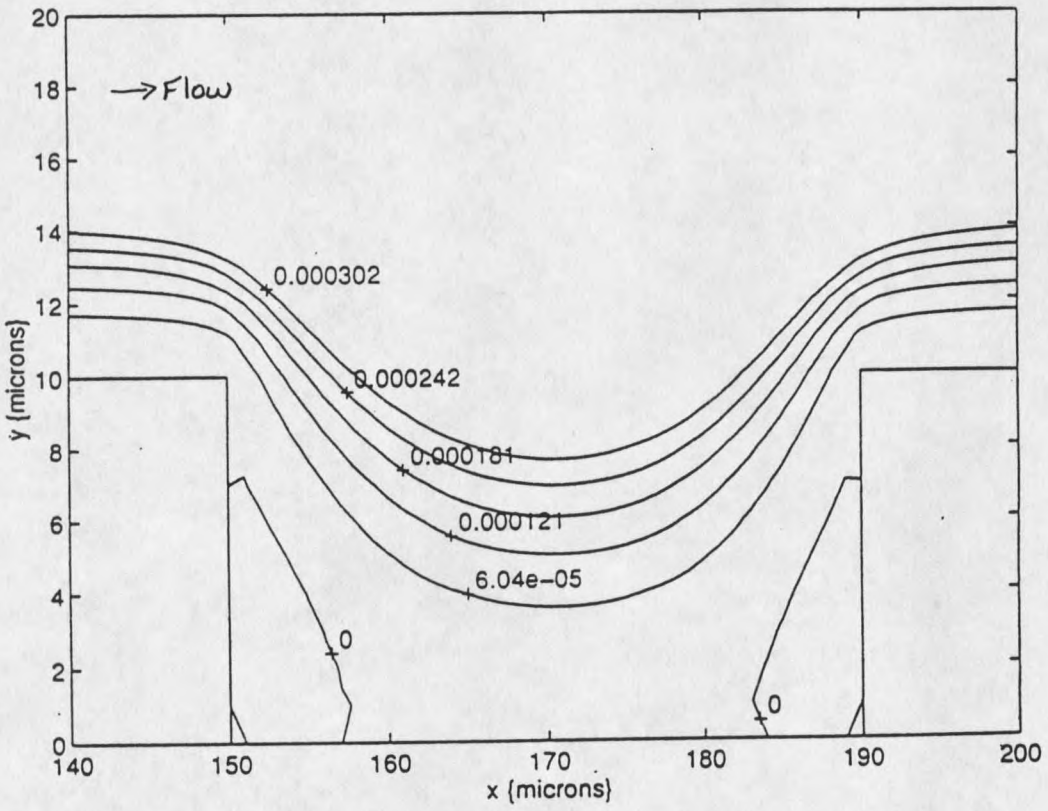

Figure 3. MMP Model Showing Stream Functions around the Cross-section of a Groove 40μm Wide and 10μm Deep. Re=6.

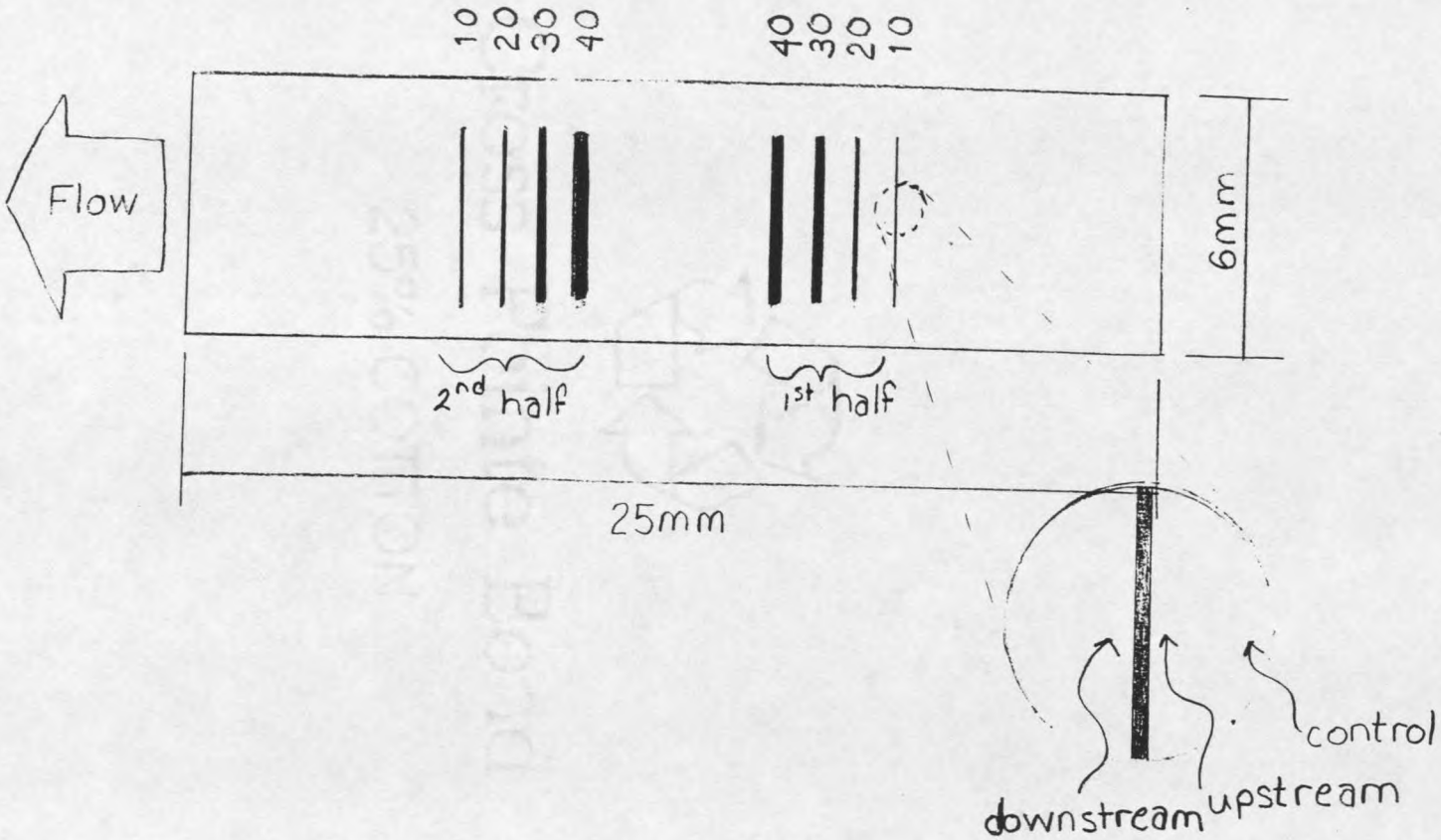

Figure 4. Schematic and Naming Convention for the Silicon Coupon.

Flow Cell and Reactor Configuration

The same parallel plate flow cell, flow conditions and cell growth rate used in this work were used in a previous study with stainless steel coupons (Camper et al. 1994). Figure 5 illustrates the parallel plate flow cell. The silicon coupon fit flush with the bottom plate of the flow cell after it was inserted into a recessed well. The top plate of the flow cell was a glass coverslip (24X60 size 1) that served as an observation window. To prevent settling effects, the flow cell was inverted and an inverted confocal laser scanning microscope was used for in-situ adhesion observation. Flow conditions were maintained at a Reynold's number of 5.5 (average velocity = 2.78 cm/s, average shear stress = 0.83 N/m^2) for all except one of the experiments. This experiment was conducted at a Reynold's number of 16.6 (average velocity = 8.33 cm/s, average shear stress = 2.5 N/m^2) to determine the effects of a higher velocity.

Figure 6 shows a schematic of the entire reactor system. The system consists of a chemostat (480 mL working volume), stir plate, air pump, mixing chamber, pumps (Cole Parmer, peristaltic,1-100), parallel plate flow chamber, dampening vessel, and various tubing and connectors. These will be described in more detail below. A dampening vessel (Figure 7) was used to reduce the pulsing effect from the peristaltic pumps. The entire system was assembled on a cart so that it could be moved to and from the confocal microscope.

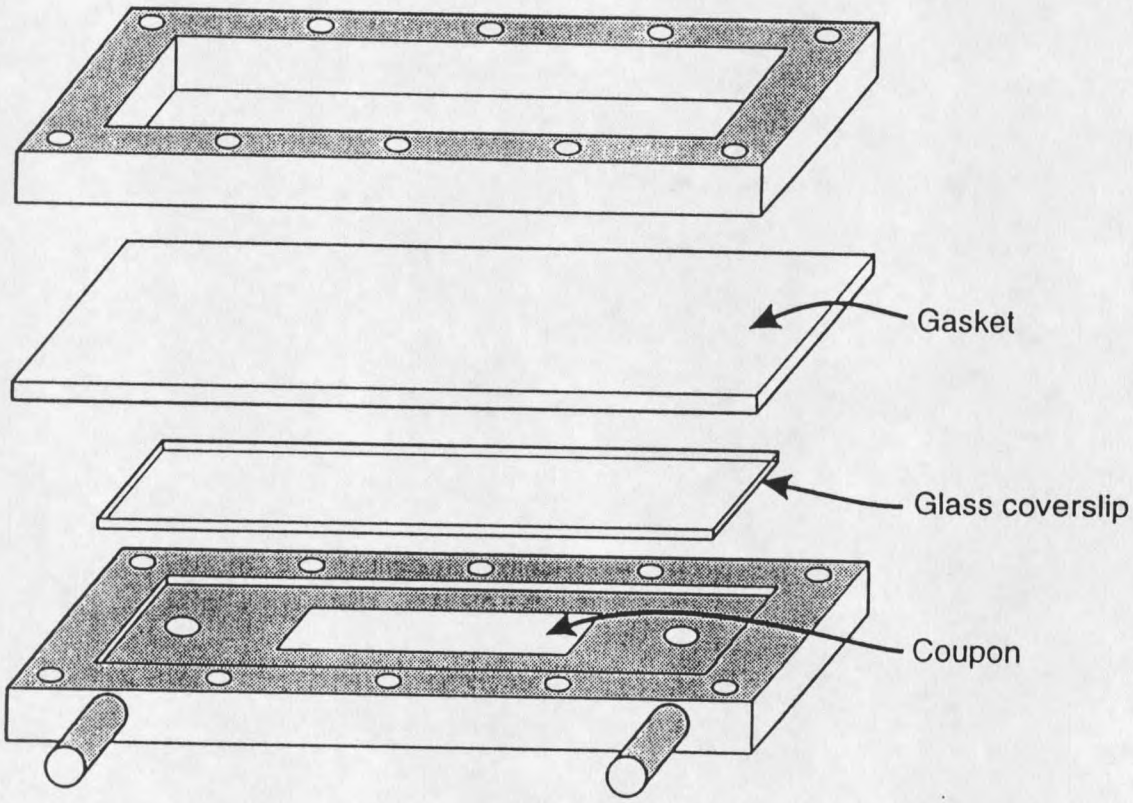

Figure 5. Schematic of the Parallel Plate Flow Cell.

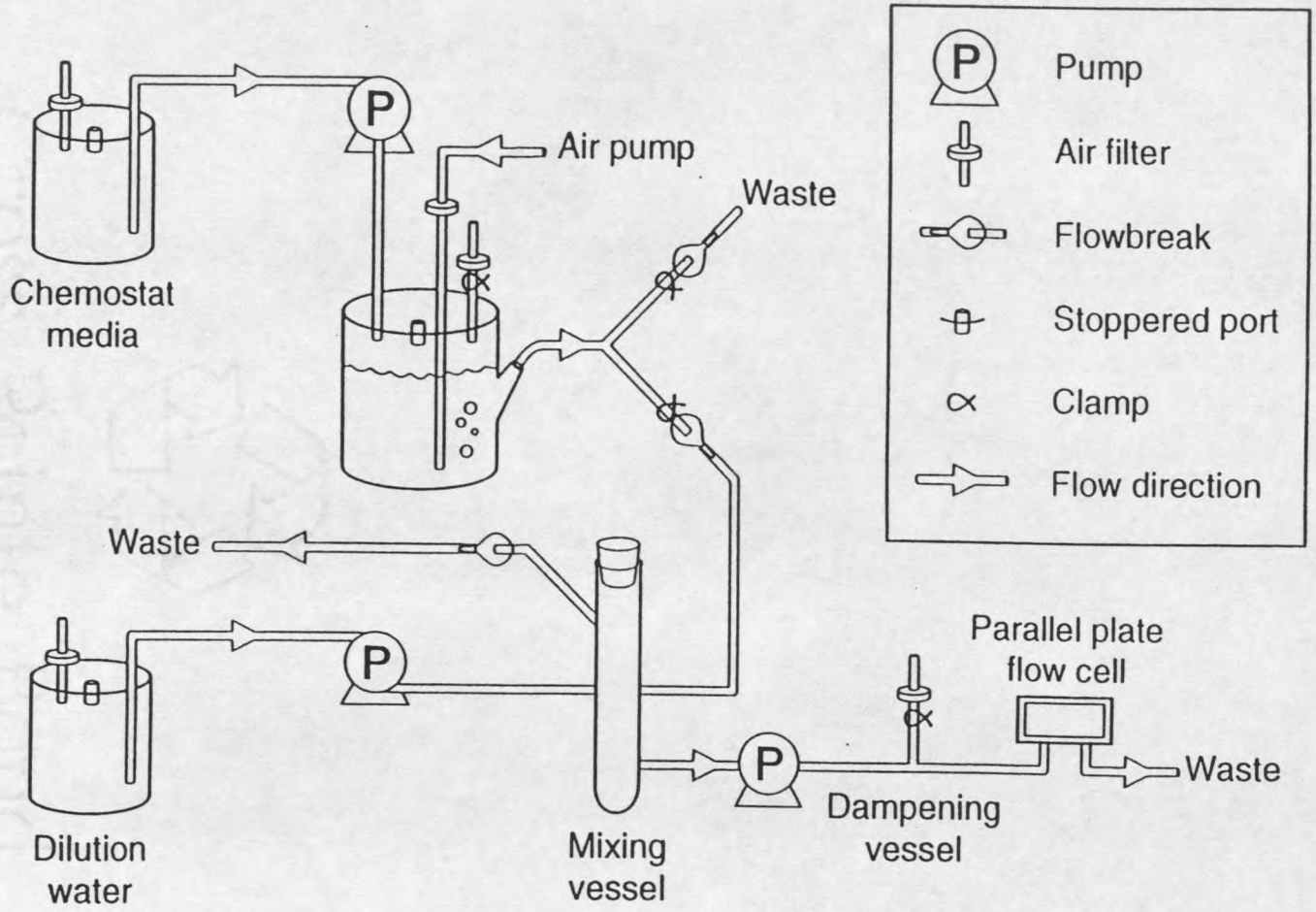

Figure 6. Schematic of the Reactor System

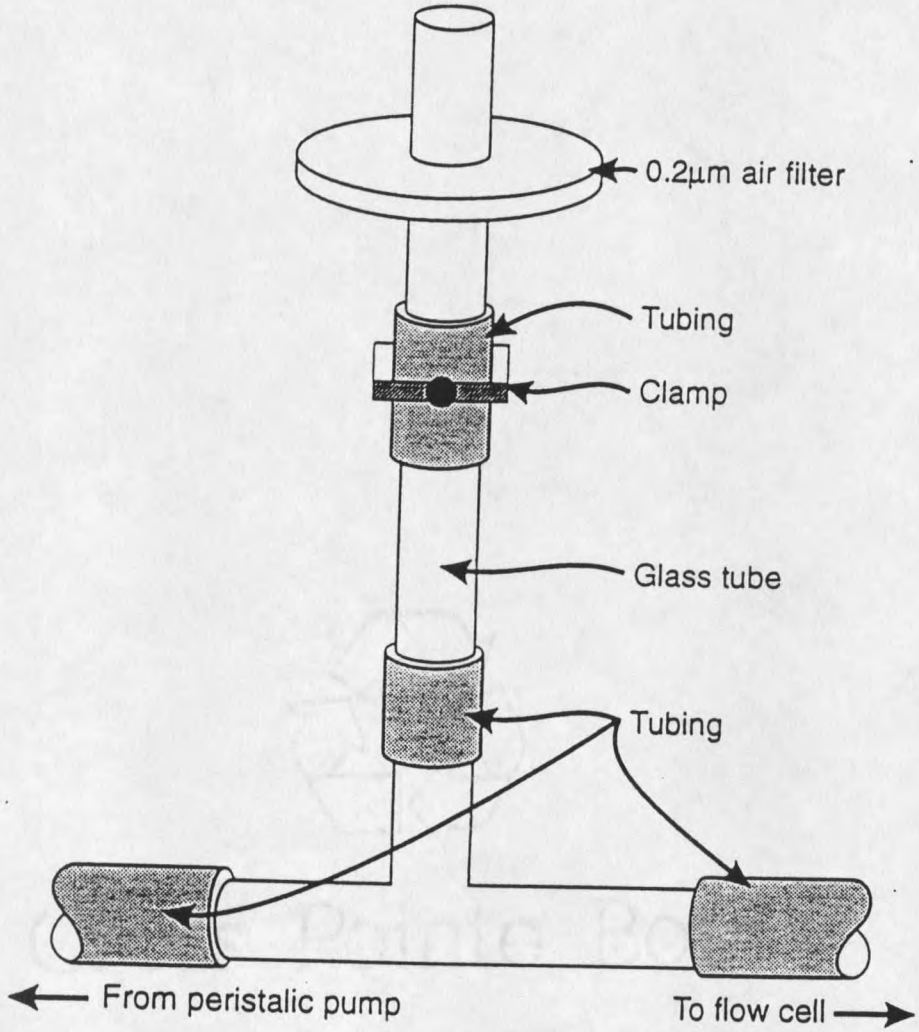

Figure 7. Schematic of the Dampening Vessel.

Organisms and Inert Particles

Three strains of aerobic, rod-shaped, gram-negative bacteria were used in the experimentation: *Pseudomonas aeruginosa (P.a.)* (ERC1 envionmental isolate in the culture collection at the Center for Biofilm Engineering, Montana State University, Bozeman, MT) *Pseudomonas fluorescens (P.f.)* (CC-8404606-E from Darren Korber, University of Saskatoon, Saskatoon, Saskatchewan, Canada) mot +, and *Pseudomonas fluorescens* mot - (nonmotile transposon). Bacterial size is 1.0 to 2.5 μm long and 0.4 to 0.6 μm in diameter. *P.a.* was used because it is well-characterized and is used often in attachment studies. It is also found quite often in aquatic environments and is a frequent contaminant of metal implants (Bisno and Waldvogel 1989). *P.f.* was used to determine the effects of cell motility. Fluorescent beads, spherical and 1μm in diameter (yellow-green carboxylate-modified that were coated with a hydrophilic polymer containing multiple carboxylic acids, Molecular Probes), were used instead of bacterial cells to document the location of attachment with respect to hydrodynamics. *P.a.* is reported to be hydrophillic (Egington et al. 1995); therefore, hydrophillic beads were chosen.

Cleaning Procedure

Tubing, Chemostat, and Carboys

The entire tubing system, including the chemostat and nutrient carboys, was cleaned between experiments by pumping bleach water through at full pump speed for

over six hours. The bleach was added to the system by introducing approximately one-half cup of bleach (5.25%) to each of the carboys filled with water. After disinfection, the system was drained and the carboys rinsed. The carboys were filled with water and the system flushed at full pump speed overnight. The system was again drained and autoclaved.

Coupon

The coupon was delivered with a protective layer of photoresist on the surface. To remove the photoresist, the coupon was immersed in acetone (Dyce Chemical, Technical grade) while the cleaning solution was prepared. The cleaning solution was "pyranha" which is composed of 70% sulfuric acid (A.C.S. Reagent Fisher Scientific) and 30% thirty percent-hydrogen peroxide (Baker Analyzed). The coupon was removed from the acetone, allowed to dry and then immersed in approximately 50mL of boiling pyranha (pyranha boils upon creation) for at least thirty minutes. The pyranha was decanted and the coupon was rinsed several times with fresh double-glass-distilled water. The coupon was placed in a Fluoroware container (composed of natural polypropylene from Flouroware, Inc.) with the cap slightly askew to dry. The cap was then closed tightly.

If the coupon appeared "dirty" to the eye (probably occurred because of dust in the air), it was cleaned again using solvents. First, it was sonicated for thirty minutes in chloroform (99.9+% HPLC grade, Aldrich) then sonicated for thirty minutes in methanol

(99.9+% HPLC grade, Aldrich). The methanol evaporated quickly and the coupon was placed in a Fluoroware container with the cap tightly closed.

The efficacy of the cleaning procedure was confirmed on selected coupons using ESCA (see Appendix A). Chemical homogeneity was confirmed by examination of the bottom of a 40μm groove and comparison with the analysis of the top plane of the coupon. A Physical Electronics Laboratories PHI-5600 ESCA spectrometer was used for the analysis. A monochromatic Al Kα source was operated at 350 watts (15kV, 23.3mA). The samples were analyzed at a 45° take-off angle which equates to a sampling depth of approximately 60 Å. The entrance aperture at the hemicspherical energy analyzer was set at 4. Pass energies for the analyzer were set at 93.90eV for wide region survey scans and 58.70eV for elemental multiplex scans (C1s, O1s, N1s, Si2p, F1s, S2p, Na1s, and Cl 2p). The operating pressure inside the main chamber was typically 5 x 10^{-8} torr. PHI ACCESS software was employed to collect and display the data and to calculate the atomic concentrations from peak area.

Glassware

All glassware used (except the carboys) was acid-cleaned in a bath of NoCromix (Cleaning solution with H_2SO_4, Godax Laboratories, NY) for at least thirty minutes, then rinsed in fresh double-glass-distilled water. The glassware was then covered in foil and placed in a 30°C oven to evaporate the remaining water. The glassware was removed and the foil was tightened.

Autoclaving Procedure

To autoclave the system, the carboys were removed and the tubing ends wrapped in paper and autoclave tape. The ends that connected tubing to the carboys were glass so that flaming could be used to achieve sterility when the carboy tubes were reattached. The reactor system (without the carboys or reactor) was autoclaved for twenty minutes on the gravity cycle (121 °C, P=23 psi). To prepare the carboys for autoclaving, the effluent tubing was clamped to prevent fluid loss during cooling. Also, the air vent was checked and changed if plugging was evident. The effluent tubing ends were wrapped in paper and autoclave tape and the caps were clamped closed with cable ties. The carboys were autoclaved for four hours on the liquid cycle (T=121 °C, P=23 psi). The reactor was not autoclaved, but was sterilized with methanol (99.9+ HPLC grade, Aldrich) immediately prior to coupon insertion.

Inoculum Preparation

Media

The chemostat media and dilution water were prepared in 9L glass carboys. The following table shows the compositions.

Table 1. Media Compositions.

Component	Chemostat Media	Dilution Water
K_2HPO_4	5.95g	5.95
KH_2PO_4	2.55g	2.55
$(NH_4)_2SO_4$	0.85g	0.85
$MgSO_4 \cdot 7H_2O$	0.085g	0.085
D-(+)-Glucose	3.4g	0

The potassium salts (Fisher) and the ammonium sulfate (Baker Analyzed) were added to the carboys which were then filled to 8.5L with RO (reverse osmosis) water and autoclaved for four hours. The magnesium sulfate (Aldrich) was added to a 250mL Erlenmeyer flask and about 150mL of nanopure water added. The glucose (Sigma) was also placed in an Erlenmeyer flask with water. Foam was placed in the necks and they were autoclaved for 20min. Prior to use, the contents of the Erlenmeyer flasks were added to the carboys through a stoppered port in the top of each carboy.

Chemostat Preparation

The sterile 480 mL chemostat was filled with chemostat media and the media pump turned off. Bacteria were injected into the septum located at the top of the chemostat and allowed to grow in batch culture for 24 hours. The stir bar was operating continuously, and air was supplied continuously. Air was allowed to escape through a 0.2μm filter at the top of the chemostat. After allowing the culture to grow in batch, the chemostat media was again turned on at a rate of 1.5 mL/min (residence time = 5 hrs)

and the chemostat was allowed to overflow to waste. The bacteria were then grown in continuous culture for 24 hours.

Cell Inoculation

Stock cultures of organisms were previously prepared in 2% peptone 20% glycerol and frozen at -70°C. Stocks were removed from the freezer and allowed to thaw to room temperature. Methanol was used to clean the septum at the top of the chemostat. A 1mL sterile syringe and needle were used to transfer the contents of the stock culture (ca. 1.5 mL) to the chemostat through the septum.

Experimental Procedure

As stated earlier, three strains of rod-shaped bacteria were used in the experimentation: *Pseudomonas aeruginosa*, *Pseudomonas fluorescens* mot +, and *Pseudomonas fluorescens* mot -. A total of nine experiments were performed. Eight of these experiments were performed at a Re = 5.5 (average velocity = 2.78 cm/s, average shear stress = 0.83 N/m^2). This Reynold's number was chosen to closely approximate the hydrodynamic modeling that was used to determine the coupon topography. The ninth experiment was performed at a Re = 16.6 (average velocity = 8.33 cm/s, average shear stress = 2.5 N/m^2). Of the low Reynold's number experiments, six of them were performed using bacteria to observe attachment behavior, one was performed using beads as a bacterial control, and one was performed using filtered chemostat effluent to determine the composition of any conditioning film.

General

After the chemostat had been operating for at least 24 hours, the entire system was moved to the confocal microscope. To prevent large loss of chemostat contents, the chemostat effluent was temporarily clamped. Power was disconnected and the system moved, after which the power was restored and the effluent clamp removed. The cleaned coupon was placed in the reactor and the flow cell was reassembled. The dilution water was turned on at a flow rate of 2 mL/min to fill the tubing and reactor to remove any air bubbles. After the reactor was mounted onto the microscope stage and the field of view was established, the chemostat effluent was redirected to the mixing chamber. The air filter at the top of the chemostat was clamped to cause mixing by forcing air into the mixing chamber. The dilution water flow was set to 1.5 mL/min and combined with the chemostat effluent (1.5 mL/min). The flow cell pump was set at 2 mL/min, allowing for overflow from the mixing chamber. Direct cell counts were performed on the reactor effluent to document the cell concentration crossing the coupon.

Images of the attached cells were then collected (artificial white light created with a combination of red, blue, and yellow wavelengths) in real time under flowing conditions and analyzed. The details of this procedure follow.

Because it was impossible to distinguish cells from the bottom of the groove, it was necessary to perform a destructive endpoint sample. To accomplish this, 0.1mL of acridine orange (see direct cell counts for source and concentration) was added to the

mixing vessel and the system was set to continuous recycle by turning the chemostat to waste and recycling the reactor effluent. After one half hour images were taken (blue and yellow wavelengths) along the top surface centered over the grooves as well as focused down into the grooves.

High Velocity

To keep the cell concentration approximately the same as the low velocity experiments (10^8 cell/mL) and to keep the cells in the same state (i.e., the same growth rate), a second chemostat was added to the system. Both chemostats were inoculated simultaneously. Everything was performed as described above except that the two chemostats and the dilution water emptied into the same mixing vessel. Also, the dilution water flow was increased to 3mL/min and the reactor flow rate was increased to 6.0 mL/min.

Bead Control

Fluorescent beads (carboxylate modified microspheres, 1μm diameter, Molecular Probes, Inc.)were used instead of bacterial cells to document the location of attachment with respect to hydrodynamics independent of biological effects. The beads were diluted to a concentration approximately equal to the concentration of cells (10^8-10^9) used in the previous experiments. A fresh coupon was inserted into the reactor. At this point, the system consisted only of the reactor pump, the reactor, the dampening vessel, and the tubing. Water was run through the system at a flow rate of 2 mL/min and the confocal microscope focused on the coupon surface. The beads were then pumped through the

system. After a full residence time (four minutes) the system was set to continuous recycle. Images were taken to document the location of attached beads over time.

Direct Cell Counts

Dilution tubes were prepared, each containing 9.0mL sterile Dulbeccos's Phosphate Buffered Saline (Sigma). Effluent was captured from the reactor after flowing over the coupon. One mL of the effluent was added to a dilution tube and the contents vortexed. Serial dilutions were made until a suitably dilute concentration was achieved. Stain (0.1% Acridine Orange in 4% formalin) was then added in 0.1mL amounts to each tube. The contents were vortexed, allowed to stand in the dark for at least 30 minutes, filtered onto a Poretics polycarbonate membrane (0.2 μm black filters, Fisher), and rinsed with nanopure water. A microscope slide was prepared by placing a drop of immersion oil on the slide. The filter membrane was placed onto the drop of oil, covered with another drop of oil and a coverslip was applied. Counts were made using an Olympus BH-2 epifluorescent microscope (BP 490 filter, 490 nm, magnification = 1000X).

Data Collection

Images were collected approximately every 20-30 min (3hrs for non-motile organisms) with an inverted Biorad Confocal Scanning Laser Microscope (MRC 600) using a 50X ULWD objective at a zoom of 2.0. Figure 8 shows schematically how the images were taken across the top of the coupon. The images were, however, taken in the same horizontal line. The first image was taken just upstream of a groove. The

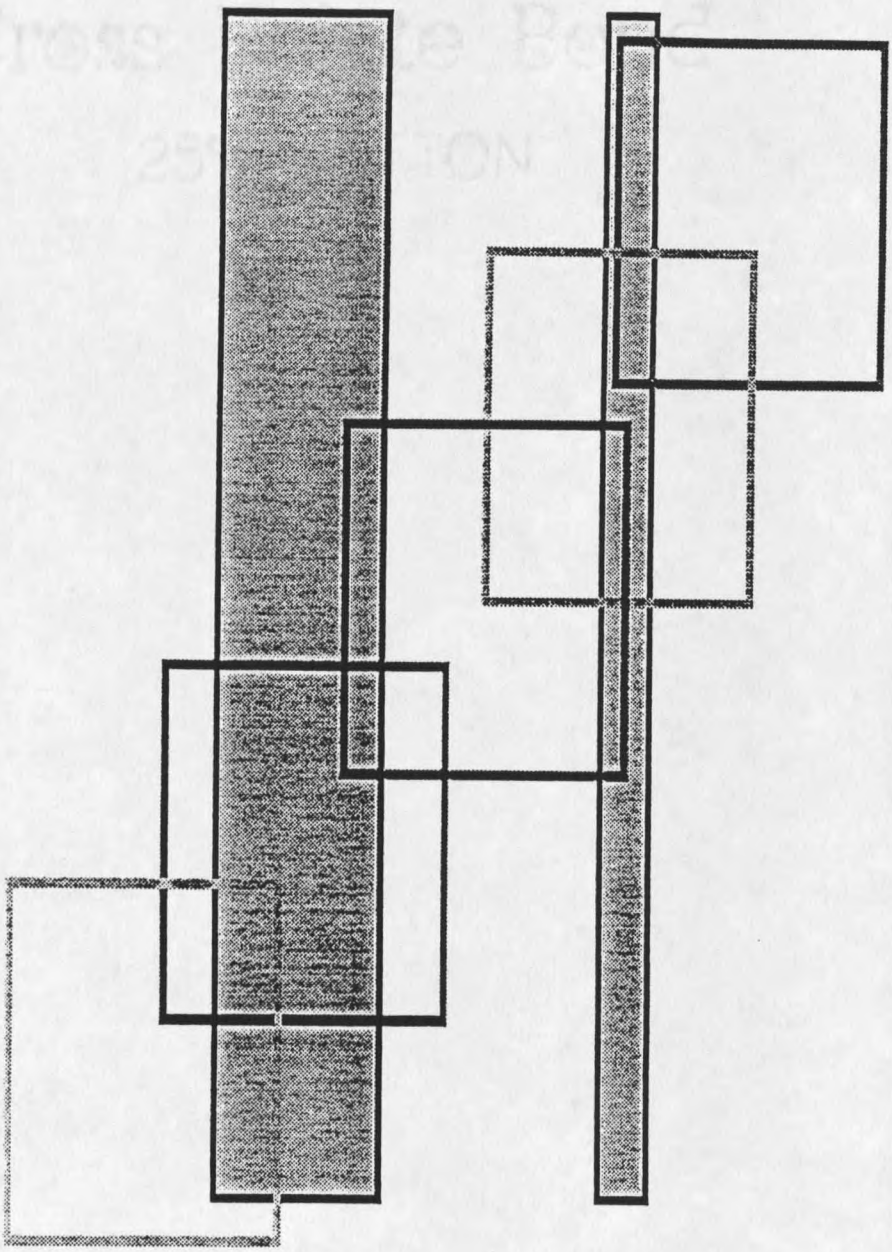

Figure 8. Schematic of How the Confocal Microscope Images Were Taken across the Coupon.

second one was taken centered over the groove. The third one taken between two grooves, and so on. At the next time period, the whole process was repeated. Notice that the edge of a groove was always included in each image to allow the images to be overlayed, thus showing the attachment over time. A sample image is shown in Fig. 9.

Conditioning Film

To document the composition of any conditioning film, the system was modified to consist only of the reactor, reactor pump, dampening vessel, and tubing. A fresh coupon was inserted into the reactor and dilution water was allowed to flow over the coupon at a flow rate of 2 mL/min for 30 minutes. Without introducing an air-water interface, the flow was switched to 0.4μm filtered *P.aeruginosa* chemostat effluent. The filtered effluent was allowed to flow over the coupon for one hour. The pump was stopped and the reactor dissassembled. The coupon was immediately placed in a filtered nitrogen (99.999%) stream. This was to prevent sedimentation of effluent elements onto the coupon. The coupon was then examined using ESCA.

Image Analysis

Advanced image analysis software (MARK, developed in-house) was used to quantify attachment information. The goal was to look at coverage at fixed distances from the grooves. The alignment of the grooves was not always vertical with respect to the image. The software will rotate the image in order that the grooves be perfectly vertical. This results in the pixel columns being the same distance from the groove.

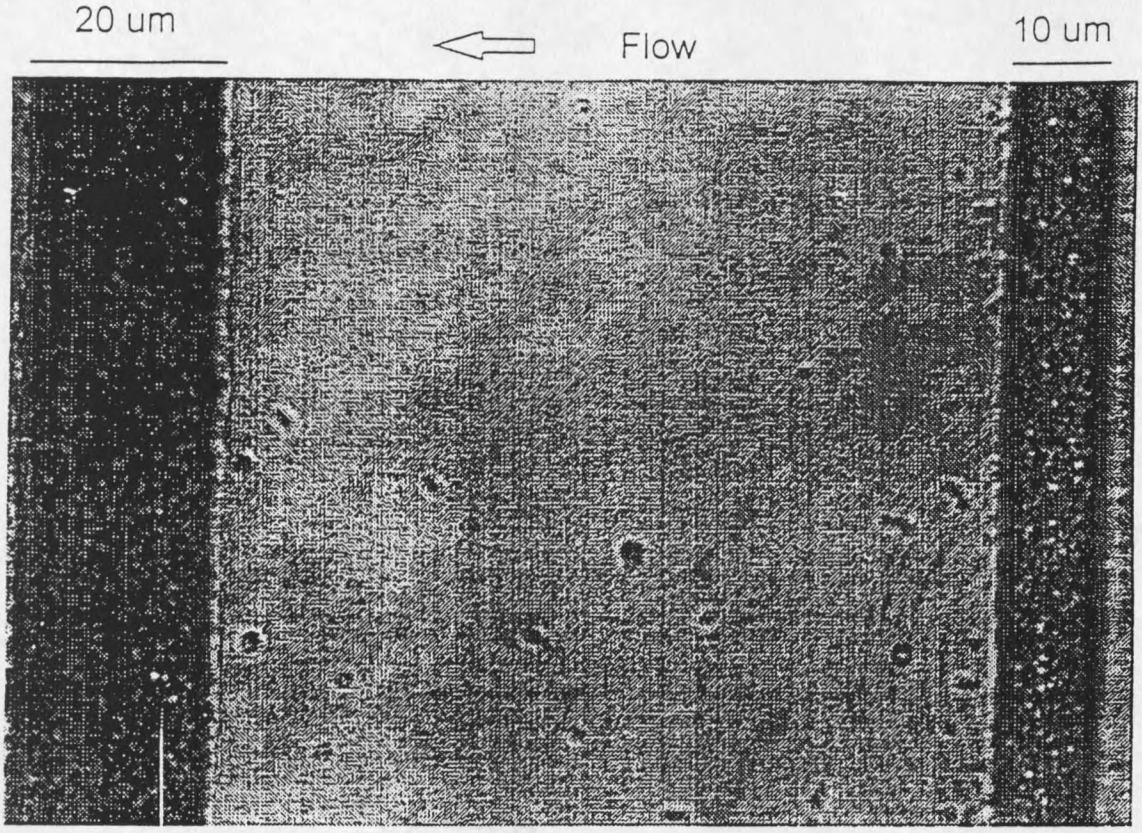

Figure 9. Sample Time Series image of *Pseudomonas fluorescens* mot+ after 0.5 Hours of Exposure to the Flow Conditions.

MARK can find the edges of the grooves and the cells with an edge finding technique. A threshold level was chosen to shade cells as black and everything else white. A manual editing feature allowed removal of the groove edge, for example, or fill the interior of a cell. For every column of pixels, now parallel to the grooves, across the image, MARK then calculated the percentage of pixels that were black (cells).

A sample plot of this raw data can be seen in Figure 10. The data are noisy because the pixel columns are at a very fine scale relative to the cell. For the time series images that were used in the data analysis, a pixel was equal to 0.165μm. To capture the trend in coverage, the data were smoothed using a statistical procedure called LOWESS (Minitab 1995) (locally weighted scatter plot smoother, f=0.4) shown in Figure 10.

Over time the same grooves were in the images taken at the same location, but because the stage was moved, they were not in exactly the same location and needed to be shifted right or left. MARK has a registration feature that allowed the groove edges to be aligned over a time series. In this way the same pixel column was the same distance from the groove edge over time. A sample is shown in Figure 11.

LOWESS showed the trend, but the entire curve could not be analyzed. Therefore, to reduce the data to a few points for statistical analysis three values were associated with the downtream edge of a groove, the upstream edge, and a control position. To account for the trend of preferential edge attachment and to reduce the amount of data, an average over 2μm was taken 6-7μm from each groove edge and at approximately 45μm from an edge. This was done for each time period for each image. These representative places are described as upstream (6-7μm upstream of a groove,

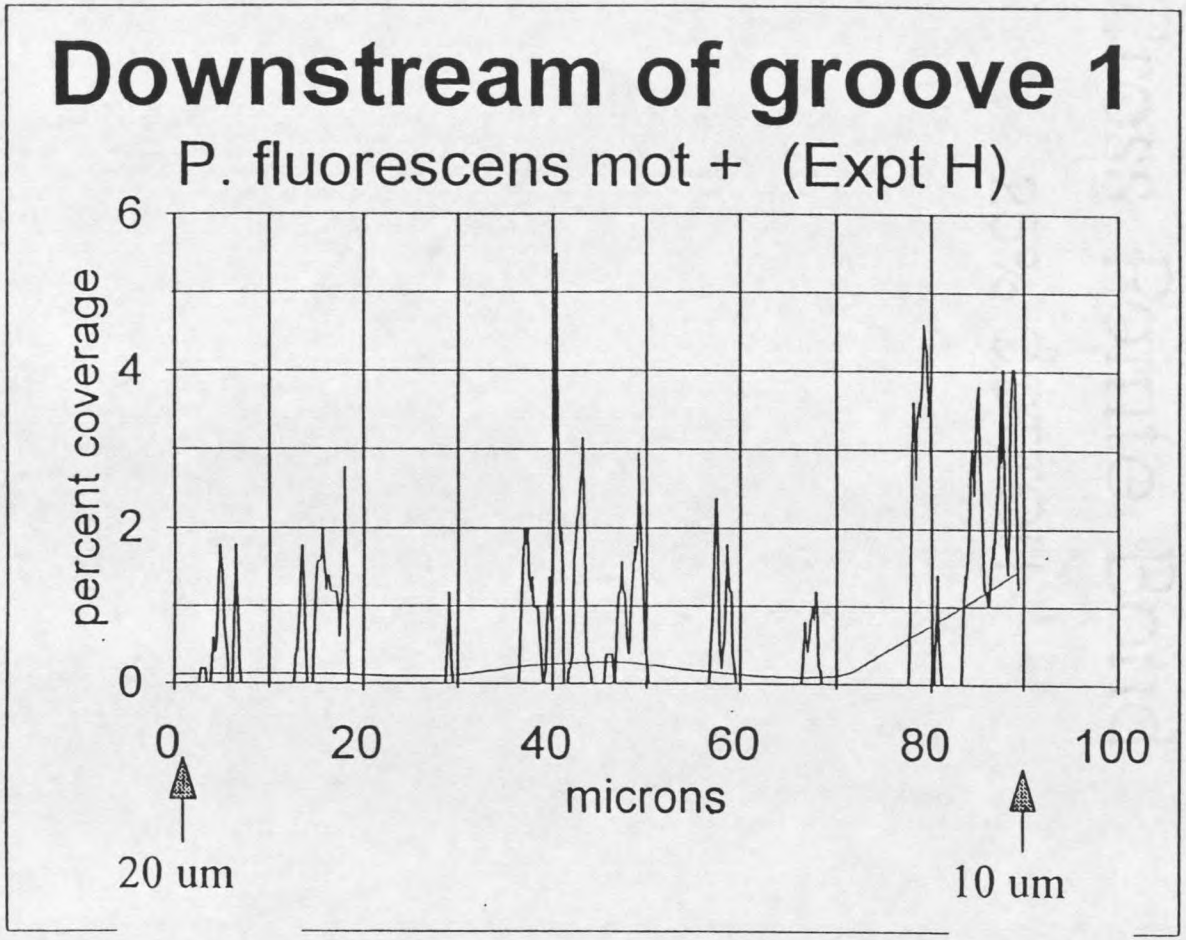

Figure 10. Sample Plot of the Raw Data from the Image Analysis Software (MARK) from the Image in Figure 9 Overlayed with a LOWESS Regression Line.

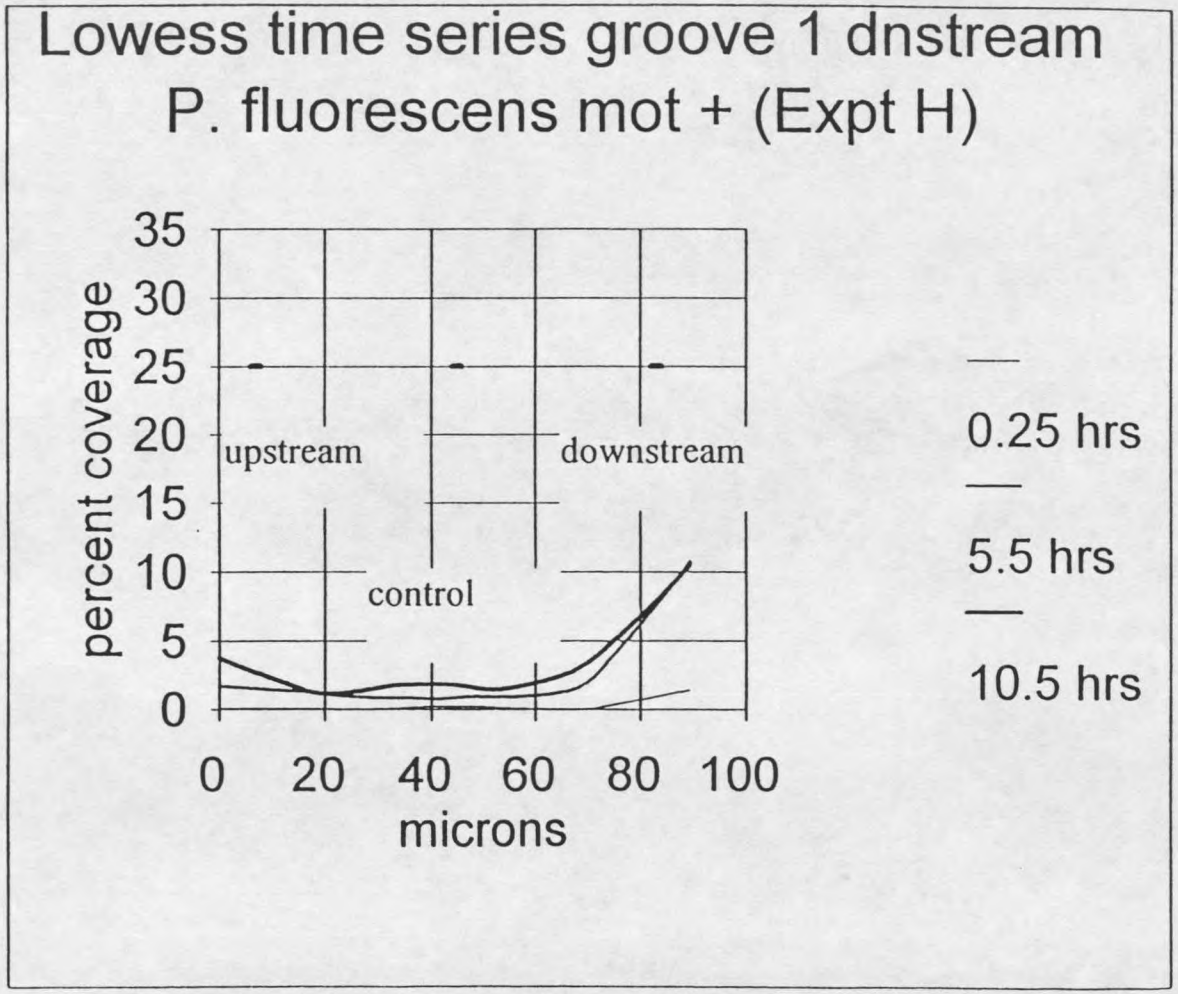

Figure 11. Sample Plot of Time Series LOWESS Lines also Showing the Positions.

downstream (6-7μm downstream of a groove) or control (45 μm from a groove - usually between grooves). These are also included in Figure 11. Note that there are two more control positions than grooves; therefore, the three positions that were associated with each groove were (1) the control upstream of the groove, (2) upstream of the groove, and (3) downstream of the groove.

Statistical Methods

Analysis of Covariance

Because the microscope was moved across the silicon coupon systematically, each microscope image was captured to a computer file at a different time. It was necessary to adjust the data for the effect of time, before assessing the effect of position, or any other factor of interest, on microbial surface accumulation. Analysis of covariance was used to accomplish that adjustment (Neter et al. 1985). The equation for the analysis of covariance model is provided in Appendix B. Note that the model contains no interaction terms. As explained in Appendix B, data analysis indicated that interactions were not important.

Briefly explained, the analysis of covariance capitalizes on the fact that $\log_{10}$(coverage) is approximately linearly related to $\log_{10}$(time) if the other factors are held constant (see Figure 12). The slope S of that linear relationship is estimated by a least squares fit to the data. Let T denote the mean of the $\log_{10}$(time) values for the experiment. Imagine a coordinate system with $\log_{10}$(coverage) on the ordinate and $\log_{10}$(time) on the abscissa. The analysis of covariance adjustment amounts to drawing a

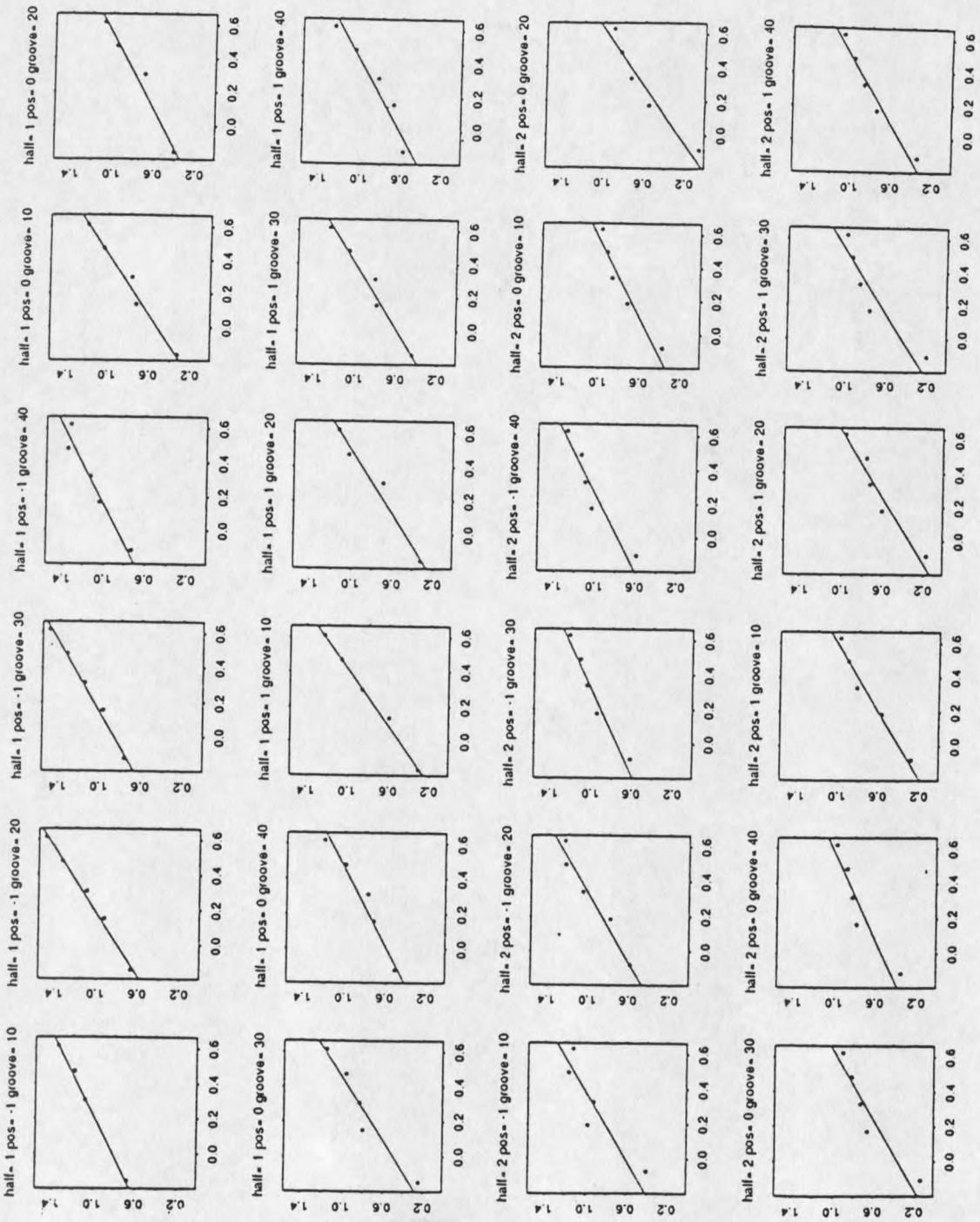

Figure 12. Sample Scatter Plot Matrix of $\log_{10}$(coverage) vs. $\log_{10}$(time) for all Combination of Factors Fitted with a Least Squares Regression Line.

line of slope S through each ($\log_{10}$(time), $\log_{10}$(coverage)) point in the data set and recording the height of the line at T. In this way each coverage is adjusted to a common time. Then a conventional analysis of variance is performed on those adjusted $\log_{10}$(coverage) values. The results pertain to a $\log_{10}$(coverage) coverage values expected at $\log_{10}$(time)=T. To test the null hypothesis that a factor (position, groove size, and half) had no effect on the mean $\log_{10}$(coverage), a conventional analysis of variance F test was used (Neter et al. 1985).

The validity of the analysis of covariance depends on assumptions about the statistical characteristics of the data. For application to coverage data, the critical assumptions are: (1) the slope S does not depend on the factor, (2) the variability of $\log_{10}$(coverage) values does not depend on the factors, (3) the distribution of $\log_{10}$(coverage) values for any time and fixed combination of factors follows a normal probability distribution, and (4) measure taken at nearly the same time are statistically independent. For each experiment the data were plotted to see if they confromed to these assumption, and they did. Figure 12 shows a diagnostic plot for evaluating (1) and Figure 13 show a diagnostic plot for evaluation of (2), (3), and (4). Figures 11-13 are examples of the plots generated for the data analysis. The plots for all seven bacterial flow experiments are included in Appendix C.

Nonlinear Regression Analysis.

The analysis of covariance provided a good way to measure the effects of the various factors on $\log_{10}$(coverage) after adjusting for the effect of time. It is of interest

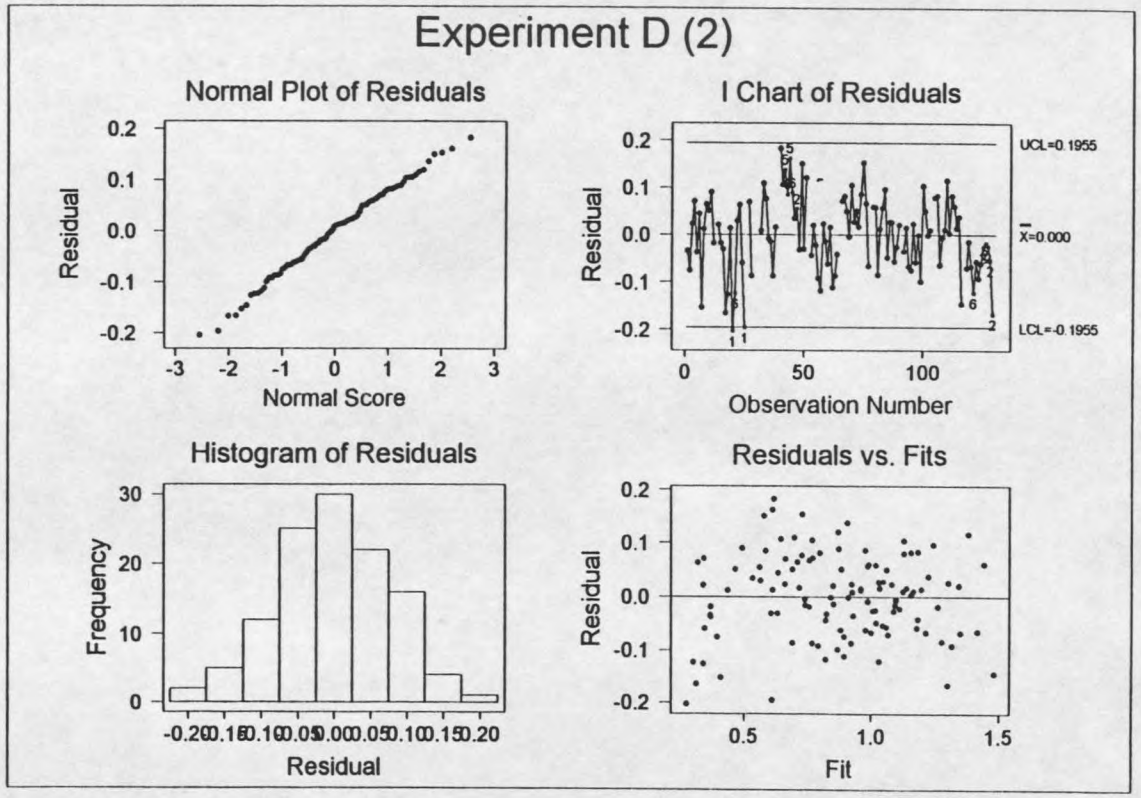

Figure 13. Sample Residual Plot to Test the Assumptions: the Variability of the $\log_{10}$(coverage) Values Does Not Depend on the Factors, the Distribution of $\log_{10}$(coverage) Values Follows a Normal Probability Distribution, and the Measures Taken at Nearly the Same Time are Statistically Independent.

to look also at surface colonization rates. The model of Equation (3) has been used by others to describe colonization as a function of time (Sjollema et al. 1989) and to calculate an initial colonization rate denoted by J. In this investigation, model (3) has been fit by nonlinear least squares to subsets of the data. The subsets were chosen according to the results of the analysis of covariance. Because the interactions between the factors were not significant, the subsets are by factor (position, groove size, and half). For each subset of data, the nonlinear least squares computer program estimated the coefficients B and J and provided an approximate standard error for each estimate. The standard error calculation is based on a local linear approximation of the nonlinear least squares predictor (Neter et al. 1989).

It was of interest to test whether two rates were statistically significantly different. To do this, an approximate t-test procedure was used. Denote the two estimates of rates to be compared by J_1 and J_2 with corresponding standard errors S_1 and S_2. Calculate the test statistic $t=(J_1-J_2)/\sqrt{S_1^2+S_2^2}$. If n_1 and n_2 data points were involved in estimating J_1 and J_2 respectively, then the degrees of freedom (df) associated with t is given by $df = \min\{n_1,n_2\}-2$. The p-values is read from tables of the Student t distribution.

Why Two Methods of Analysis.

In order to use standard statistical software for conducting the analysis of covariance, it was necessary to work on the $\log_{10}$(coverage) scale where the response

variable conformed to the assumptions of homogeneous variance and normality (assumption (2) and (3)). When the estimated nonlinear curves of model (3) were plotted on a $\log_{10}$(time) by $\log_{10}$(coverage) axis system, the curves were almost linear. For this reason, it is reasonable to believe that the linear relationship used in the analysis of covariance provided essentially the same qualitative results relative to assessing the significance of each factor (position, half, groove width, etc.) that would occur if one devised an analysis specifically built around Equation (3). As discussed in Appendix B, the analysis of covariance provided a framework for assessing potential interactions between the factors. No practical interactions were observed, a fact that allows one to study the effects of a single factor by averaging over all the data. That is, studying the factor "position" it is valid to average over all halves and groove widths. Therefore, one can legitimately compare the average effect for downstream to the average effect of control.

The importance of Equation (3) in surface colonization literature made it necessary to used Equation (3) explicitly in calculating the results. Because there were no apparent interactions between factors, it was valid to estimate the model for downstream position, say, using all downstream data in the experiment, regardless of half or groove width. Thus the analysis of covariance guided the manner in which the data were subsetted when estimating the J and B of Equation (3).

RESULTS

Experimentation Summary

Nine experiments were performed in this research, including seven flow experiments with bacteria, one control using beads and one using filtered chemostat effluent to study the deposition of a conditioning film (see Table 2).

Table 2. Summary of Bacterial Flow Experimentation.

Experiment	Organism	Motility	Reynold's Number
A (1)	*P. aeruginosa*	Motile	5.5
D (2)	*P. aeruginosa*	Motile	5.5
E (6)	*P. fluorescens*	Non-motile	5.5
H (4)	*P. fluorescens*	Motile	5.5
J (3)	*P. fluorescens*	Motile	5.5
K (5)	*P. fluorescens*	Non-motile	5.5
N (7)	*P. aeruginosa*	Motile	16.6
O	beads	N.A.	5.5
P	none conditioning film	N.A.	5.5

Each of these experiments was performed in a parallel plate flow chamber with a fresh coupon. The experimental results will be given for the seven bacterial flow experiments, followed by the bead control, and finally for the conditioning film study.

Bacterial Flow Experiments

Summary

Qualitatively, the results of the experiments with bacteria indicate that there is preferential attachment to the downstream edge of the grooves. It did not appear that the groove size was influential in the rate of attachment. Also, there appeared to be a difference in the rate of attachment between the two motile strains, even though they were grown under the same conditions. The nonmotile cells attached much slower than the parent motile strain and there was a strong degree of clumping or aggregation upon attachment. From the fluorescent images, it was observed that the motile organisms adhered as readily to the bottoms of the grooves as they did to the tops. The nonmotile strain, however, rarely attached in the bottoms of the grooves.

Statistical Results (generalized)

In order to determine the significance of the groove size, position (upstream, downstream, or control), half (first or upstream vs second or downstream), velocity, motility, or species on the rate of attachment, two methods to analyze the data were used as described in the Materials and Methods section. Following is a summary of the general information gained from the analysis of covariance (The specific results of both the analysis of covariance and the nonlinear regression analysis will be described in more detail in the Experimental Results section.).

Separating the data into sets for half (first vs. second), groove size, or position (upstream, downstream, or control) for each experiment, it was possible to determine the significance of each of the 3 factors within each experiment (The analysis of variance, ANOVA, results are included in Appendix C). This analysis also indicated that there were no interactions between these three effects (See Appendix B). Table 3 (The tables and figures in this section will be collected at the end for the reader's convenience as many of them will be referenced repeatedly.) shows the p-values associated with each of the ANOVA runs. It can be seen that only Experiments 1 and 4 show that the groove size is significant ($p=0.016$ and $p=0.002$ respectively). Because the p-value for Experiment 1 was relatively high, and because Experiments 1 and 2 were replicates, the data for Experiments 1 and 2 were combined and the effect of groove size was no longer significant ($p>0.05$). A plot was made of the data in Experiment 4 by groove and there was no trend by groove size. Therefore, the effect of groove size was determined to be insignificant on the rate of attachment. In contrast, the effect of position was always significant except for Experiment 6 ($p=0.2$) which had very little attachment even after 12 hours (<5% coverage). The effect of half was significant only for the motile organisms.

Bacterial Flow Experimental Results

Because this section deals with each experiment independently, the results will be ordered by organism as follows: *Pseudomonas aeruginosa* including the high velocity experiment, *Pseudomonas fluorescens* mot +, and *Pseudomonas fluorescens* mot -. At

the end of the *P.aeruginosa* section, the effects of a higher velocity will be explored. The effects of the strain dependency of the motile organisms will appear at the end of the *P. fluorescens* mot + section, and the effect of motility will be explored at the end of the *P. fluorescens* mot- section.

Pseudomonas aeruginosa. Figure 14 is a representative image of these data and is a merge of two end-point fluorescent images - one of the top plane and one of the bottom plane. Notice the strong downstream edge effect and that there are as many cells in the bottoms of the grooves as there are in the control positions on the top plane.

The p-values for the ANOVA results for Experiment 1 (from Table 3) show that half and position are significant. Table 4 lists the J and B values from the exponential model. Figures 15 and 16 show plots of the exponential model using these J and B values. From Figure 15 we can see that attachment is faster on the first half than on the second half. Figure 16 shows that the rate for the downstream edges is much faster than for the upstream edges which is slightly higher than for the control positions. Individual data points vary considerably from the model, but the model tracks the time trend quite well. To show this, the data points for the first half were plotted on the plot by half, Figure 15, and the data points for the downstream edges were plotted on the plot by position, Figure 16. The data points for the first half and downstream edges are displayed on the plots for all seven experiments. Note that in all these plots, the variability of the coverage points increases with time.

Table 3 shows that position is significant. Further, Table 5, a summary of t-tests, shows the significance of each pair of positions. The downstream edges have a statistically significantly higher rate of attachment than the control positions. Downstream compared to upstream and upstream compared to control are not statistically significant. However, a ratio of the rates of attachment (as shown in Table 5) show that the rate of attachment is highest on the downstream edges, followed by the upstream edges, and lowest at the control positions.

Experiment 2 shows very similar results to Experiment 1. The ANOVA runs show that all three effects (position, half, and groove) are significant. However, as explained earlier, the effect of groove size seems to be a statistical artifact. Figures 17 and 18 show the resulting exponential curves. These curves are similar in shape to Experiment 1. Again, the rate for the first half was higher than for the second half. Also, the downstream edges had a statistically significantly higher rate than for the upstream edges and for the control positions (Table 5). The control positions and the upstream edges rates were very nearly the same as shown by the ratio in Table 5.

Table 6 shows the inter/intra experiment variability between Experiments 1 and 2. The variability within experiments is higher than the variability between the two experiments. This means that there is good reproducibility between replicate experiments for the flow cell methodology.

Experiment 7, the higher velocity experiment, shows the same trends as Experiments 1 and 2 with the first half showing a significantly higher rate than the second half as well as the rates for the positions following the same order: downstream >

upstream > control (Figures 19 and 20 and Table 4). The analysis of covariance indicated that the position effect was significant on the rates of attachment. However, Table 5 shows that none of the combinations are significant. This should not be viewed as contradictory since they were based on different measures; the ANOVA results were based upon the log values adjusted to a mean time, whereas the t-test results were based upon the J values. We can see by the plot in Figure 20 that the initial rates are very nearly the same, but the final coverages have different plateau values. Therefore, even though position was not a statistically significant effect, the rates of attachment were highest on the downstream edges and lowest at the control positions. When compared to the Re = 5.5 experimental data, it is also obvious that the position effects in the higher velocity experiment were not as pronounced.

To see whether increasing the fluid velocity had a significant effect, compare the results from the t-tests shown in Table 6. With only one exception, the initial rate of attachment for the high velocity experiment (Experiment 7) is greater than the rate for the low velocity experiments. Only about half of the ratios are statistically significant, but because of the consistent trend, the conclusion is that the initial rate of attachment is greater for the higher velocity experiment. By comparing the J/B values for Experiments 1, 2, and 7 we can see that the plateau values (J/B) are higher for Experiments 1 (12.3 and up) and 2 (18.6 and up) than for Experiment 7 (5.5 - 9.0).

Pseudomonas fluorescens mot + Two representative images from these experiments are shown here, with Figure 9 (Materials and Methods) representing a time

series image and Figure 21 showing a merge of two fluorescent images. Notice that there is a strong downstream edge effect and that there are cells in the bottoms of the grooves.

The ANOVA results for Experiment 3 are given in Table 3. In this experiment, only the half made a difference on the rate of attachment. As shown in Figure 22, there was greater coverage for the second half than the first half. This result is opposite the *P. aeruginosa* data which showed a higher rate of attachment on the first half than the second half. Position is not shown to be significant and Figure 23 shows the lines nearly superimposed. Note the large p-values for this experiment shown in Table 5. In this experiment there was not a downstream edge effect.

The ANOVA results for Experiment 4 show that all three effects were significant. The effect of groove size was judged to be a statistical artifact as explained earlier. A plot of the results by half show that again (Figure 24), the rate of attachment is higher on the second half than the first half. This is in agreement with Experiment 3. Position is shown to be significant in the ANOVA (Table 3) results but not in the t-tests (Table 5). This is probably because of the extremely high standard errors of the J values shown in Table 4. Looking at the plot of the coverage by position, Figure 25, it is clear that the rate of attachment is much higher for the downstream edges than for the upstream edges or control positions.

Table 9 shows that there is not much variability between replicate experiments compared to the variability within the experiments. The ratio of the two values confirms this, showing that there was good reproducibility for the flow cell experimental methods.

Table 7 shows the results of the t-test comparing data from the four experiments using motile strains at Re=5.5. Generally, the rate is higher for *P. aeruginosa* than for *P. fluorescens mot* +. This analysis is complicated by the fact that the J values for experiment 4 were high for the downstream and control positions and were accompanied by high standard errors.

Pseudomonas fluorescens mot - Representative images are shown of this strain as well. Figure 26 shows a time series image taken after much longer time (15 hours) than in the previous experiments with motile bacteria. Also, notice the aggregation. Based on direct observation, the cells do not come to the surface as clumps but upon attachment, form larger and larger aggregates. At this time, there is probably growth occurring as well. Figure 27 shows an end-point fluorescent image taken after 21 hours exposure to the bacterial suspension. There are no cells in the bottoms of these grooves. Figure 28 shows another image after the magnification was lowered. Note that there are a significant number of aggregates and that they tend to be located along the downstream edges. Because this work concerns the initial events of biofilm formation, the data analysis for Experiments 5 and 6 was truncated to times less than 12 hours.

The ANOVA results for Experiment 5 (Table 3) show that only position is significant. The positions are all statistically significantly different as shown in Table 5. The plot in Figure 30 shows that the rate of attachment is greatest along the downstream edges and lowest for the control sections of the coupon. Half was not important since the plots in Figure 29 are superimposed.

Experiment 6 did not have much coverage at all, even after long times of 46 hours. The ANOVA results in Table 3 show that there are no significant effects. Figure 31 shows the two curves for coverage with regards to coupon half nearly superimposed. The trend with the rate of attachment being highest for the downstream edges and lowest for the control sections does not follow and the downstream edges show the lowest rate of attachment as can be seen in Figure 32. However, because of the extremely low coverages, data from this experiment should be viewed with caution.

The comparison between the two experiments in Table 9 again shows good reproducibility in the experimental method. The total variability was the least for Experiments 1 and 2 and the most for Experiments 5 and 6.

Table 8 shows the results of the t-tests to determine if motility was a significant factor. It has already been pointed out by reference to the representative images that the rates are lower for the nonmotile strain than for the motile strains. Experiment 3 has a statistically higher rate of attachment than Experiments 5 and 6. Even though not statistically significant, Experiment 4 had a higher rate of attachment than Experiments 5 and 6. Therefore, motile *P.f.* has a higher initial rate of attachment than nonmotile *P.f.*

Summary To summarize the results of the bacterial flow experiments, the following was found (1) replicate experiments showed greater variability within each experiment than between the two experiments, (2) *P. aeruginosa* has a higher rate of attachment than *P. fluorescens* mot + which has a higher rate of attachment than *P. fluorescens* mot -, (3) the rate of attachment was found to be independent of the groove

size, (4) the rate of attachment was greatest on the downstream edges of the grooves and least at the control sections, (5) the rate of attachment was highest on the first half of the coupon for some of the experiments and on the second half for others, (6) the nonmotile organisms showed evidence of clumping or aggregation, (7) only the motile organisms were found in the bottoms of the grooves, (8) an increase in the fluid velocity results in a corresponding increase in the rate of attachment (with identical cell concentrations), and (9) an increase in the fluid velocity results in a decrease of the impact of position.

Bead Experiment

A representative image is shown in Figure 33. Recall that the same concentration of beads was used as was cells in the previous experiments. This image was taken after about 5 hours. The experiment was left overnight and the coverage did not change appreciably. It appeared that if the beads appeared on the surface, they were irreversibly attached. It was expected that the beads would behave similarly to the nonmotile bacteria. It is clear that there was not an edge effect and that the beads did not aggregate. There were few bright spots inside the grooves indicating that the beads did not stick in the bottoms of the grooves, which was similar to the nonmotile cells.

Conditioning Film Study

The surface was analyzed with ESCA (the report is included in Appendix A) and was found to be contaminated with PDMS, poly(dimethylsiloxane). PDMS on the

coupon surface is probably from the vacuum grease used to hold the coupon down in the bottom plate of the parallel plate flow cell. Also, there was a small amount of organic nitrogen on the surface of the silicon coupon suggesting that a very thin film of macromolecules was present on the surface as a conditiong film. The film was either very thin or discontinuous because the silicon substrate was also observed. The organic film is no greater than 100Å thick because the amount of nitrogen was only about 4%. A thick film in contrast, contains between 11 and 15% nitrogen (Schamberger report included in Appendix A). Evidence of potassium and phosphorus from the buffer solution was also found on the coupon.

Table 3. Analysis of Covariance p values

	Experiment Number						
Factor	1	2	3	4	5	6	7
half	0.001	0.000	0.018	0.000	0.393	0.974	0.000
position	0.000	0.000	0.252	0.000	0.000	0.200	0.001
groove	0.016	0.000	0.903	0.002	0.054	0.144	0.213

Note: The p-value is for the null hypothesis that the factor has no effect on the mean response (log coverage).

Table 4. Least Squares Estimates and Associated Standard Errors for the Parameters of the Exponential Model (Eq. (3)) or the Linear Model for Selected Subsets of the Data.

		exponential model				linear model	
Data		j	std error	b	std error	J	std error
Expt 1	half 1	4.033	0.923	0.164	0.159		
	half 2	3.001	0.975	0.147	0.215		
	pos -1	5.573	1.092	0.209	0.137		
	pos 0	2.408	0.553	0.195	0.160		
	pos 1	3.218	0.973	0.231	0.218		
Expt 2	half 1					4.520	0.202
	half 2	4.694	0.722	0.252	0.109		
	pos -1	6.908	1.011	0.142	0.094		
	pos 0	3.211	0.437	0.089	0.083		
	pos 1	3.326	0.498	0.015	0.086		
Expt1&2	half 1	3.735	0.578	-0.034	0.089		
	half 2	3.883	0.630	0.211	0.112		
	pos -1	6.062	0.827	0.146	0.089		
	pos 0	2.823	0.442	0.094	0.099		
	pos 1	3.019	0.494	0.050	0.010		
	groove 10	4.430	0.946	0.195	0.146		
	groove 20	3.721	1.005	0.052	0.164		
	groove 30	3.796	0.856	0.044	0.136		
	groove 40	3.752	0.966	0.107	0.164		
Expt 7	half 1	11.750	2.910	1.300	0.547		
	half 2	3.798	0.759	0.592	0.333		
	pos -1	10.111	4.331	1.253	0.916		
	pos 0	5.693	1.963	1.034	0.683		
	pos 1	8.915	2.986	1.351	0.739		
Expt 3	half 1	1.572	0.234	0.447	0.094		
	half 2	2.043	0.308	0.301	0.076		
	pos -1	1.613	0.333	0.223	0.091		
	pos 0	1.837	0.294	0.414	0.091		
	pos 1	2.015	0.538	0.477	0.180		
Expt 4	half 1	0.502	0.437	0.096	0.220		
	half 2	0.943	0.862	0.057	0.211		
	pos -1	13.298	10.594	1.470	1.223		
	pos 0	2.718	3.365	1.177	1.507		
	pos 1					0.531	0.082
Expt 5	half 1					0.419	0.076
	half 2					0.444	0.063
	pos -1					0.790	0.091
	pos 0					0.160	0.018
	pos 1					0.344	0.067
Expt 6	half 1	0.493	0.615	0.479	0.689		
	half 2					0.124	0.014
	pos -1					0.093	0.022
	pos 0	0.259	0.202	0.102	0.189		
	pos 1	0.112	0.065	0.039	0.117		

Table 5. T-test Results to Determine the Significance of the Factor: Position.

Expt		Ratio	t	p
1	dwn, cntrl	2.314	2.586	0.006
	cntrl, up	1.336	0.724	0.236
	dwn, up	1.732	1.610	0.056
2	dwn, cntrl	2.151	3.357	0.001
	cntrl, up	1.036	0.172	0.432
	dwn, up	2.078	3.179	0.001
3	dwn, cntrl	0.878	0.504	0.693
	cntrl, up	1.097	0.290	0.386
	dwn, up	0.800	0.635	0.737
4	dwn, cntrl	4.893	0.948	0.173
	cntrl, up	0.197	0.648	0.741
	dwn, up	24.810	1.205	0.116
5	dwn, cntrl	4.942	6.797	0.000
	cntrl, up	2.153	2.658	0.005
	dwn, up	2.296	3.949	0.000
6	dwn, cntrl	0.193	-0.815	0.791
	cntrl, up	0.434	-0.690	0.754
	dwn, up	0.445	-0.283	0.611
7	dwn, cntrl	1.776	0.929	0.178
	cntrl, up	1.566	0.902	0.185
	dwn, up	1.134	0.401	0.345

Ratio = J for downstream/J for control
Ratio = J for upstream/J for control
Ratio = J for downstream/J for upstream

Note: The t statistic and p-value are for the null hypothesis that the true ratio of J's equals 1.

Table 6. Comparison of the Rate of P.a. Attachment in Expt 7 (Re=16.6) to Expts 1 and 2 (Re=5.5).

	Expt 1&7		Expt 2&7	
	J7/J1	p	J7/J2	p
Half 1	2.913	0.007	2.600	0.008
Half 2	1.266	0.260	0.809	0.803
Downstream	1.814	0.156	1.464	0.237
Control	2.364	0.000	1.773	0.110
Upstream	2.770	0.037	2.681	0.034

Note: the p-value is for the null hypothesis that the true value of J is equal to 1.

Table 7. Comparison of the P.a. Attachment in Expts 1 and 2 to the P.f. mot + Attachment in Expts 3 and 4.

		J/J (P.a./P.f.)	t	p
Expt 1&3				
	Half 1	2.566	2.585	0.011
	Half 2	1.469	0.937	0.351
	Downstream	3.455	3.469	0.008
	Control	1.311	0.909	0.366
	Upstream	1.597	1.082	0.282
Expt 1&4				
	Half 1	8.034	3.458	0.001
	Half 2	3.182	1.581	0.119
	Downstream	0.419	0.725	0.471
	Control	0.886	0.091	0.928
	Upstream	6.004	2.747	0.008
Expt 2&3				
	Half 1	2.875	9.537	0.000
	Half 2	2.298	3.377	0.001
	Downstream	4.283	4.975	0.000
	Control	1.748	2.609	0.010
	Upstream	1.650	1.787	0.077
Expt 2&4				
	Half 1	9.004	8.346	0.000
	Half 2	4.978	3.336	0.001
	Downstream	0.519	0.600	0.550
	Control	1.181	0.145	0.885
	Upstream	6.203	5.526	0.000

Note: the t statistic and p-value are for the null hypthosis that the true ratio of J's equals 1.

Table 8. Comparison of the motile P.f. Attachment in Expts 3 and 4 the nonmotile P.f. in Expts 5 and 6.

		Jmot+/Jmot-	t	p
Expt 3&5				
	Half 1	3.750	4.685	0.000
	Half 2	0.457	5.084	0.000
	Downstream	2.043	2.385	0.010
	Control	11.496	5.694	0.000
	Upstream	5.858	3.082	0.002
Expt 3&6				
	Half 1	3.191	1.641	0.053
	Half 2	40.778	6.224	0.000
	Downstream	32.305	4.555	0.000
	Control	70.935	4.421	0.000
	Upstream	17.943	3.511	0.000
Expt 4&5				
	Half 1	1.198	0.187	0.426
	Half 2	2.124	0.578	0.283
	Downstream	16.839	1.181	0.121
	Control	17.009	0.760	0.225
	Upstream	1.558	1.817	0.037
Expt 4&6				
	Half 1	1.019	0.410	0.342
	Half 2	18.822	0.950	0.173
	Downstream	266.333	1.247	0.109
	Control	10.495	0.729	0.234
	Upstream	4.773	4.066	0.000

Note: the t statistic and p-value are for the null hypothesis that the true ratio of J's equals 1.

Table 9. Variance Component Analyses (based on log Coverage).

Experiments	1&2	3&4	5&6
Variance between	0.014	0.005	0.053
Variance within	0.029	0.361	0.490
var between/var within	0.650	0.014	0.110

Note: total variance = variance between + variance within

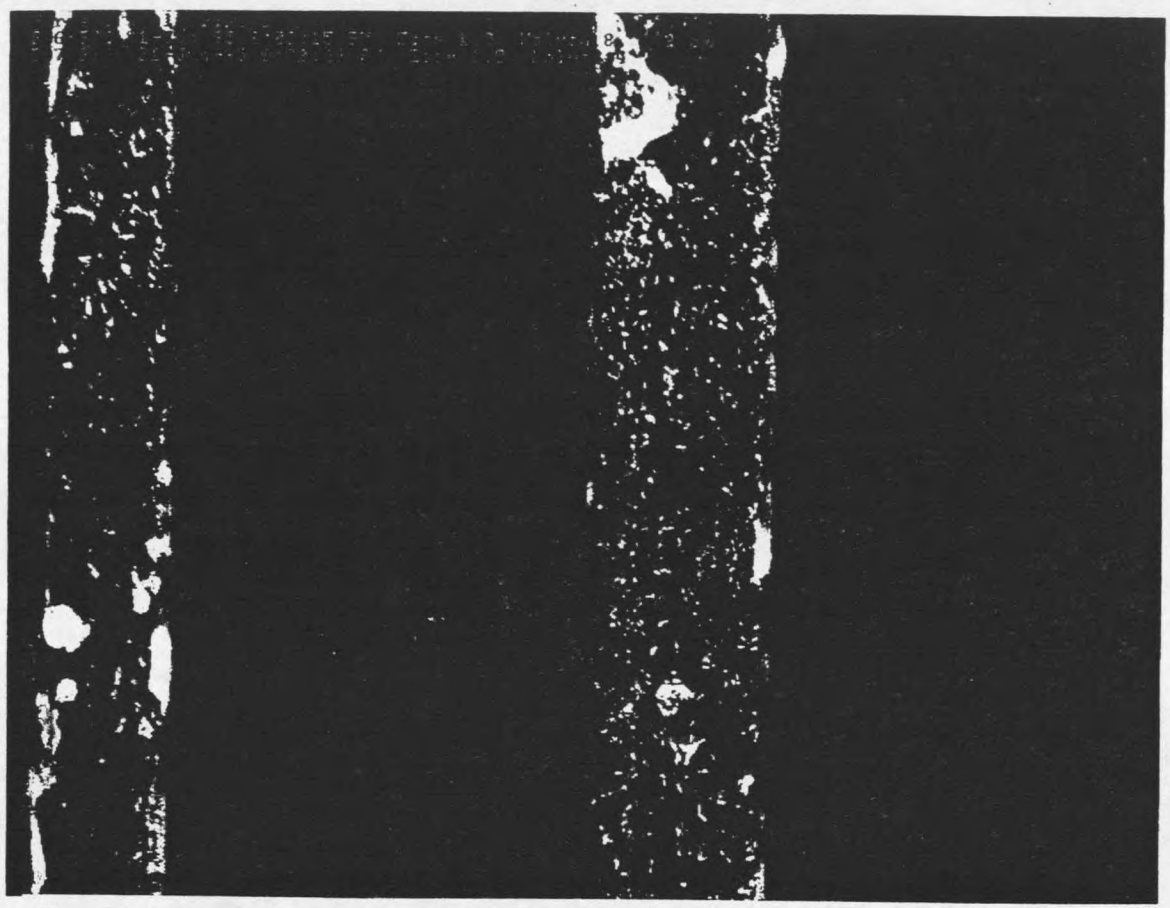

Figure 14. Representative End-point Fluorescent Image of *Pseudomonas aeruginosa* Taken after 5.5 Hours of Exposure to the Flow Conditions. This figure is a merge of two images: the light colored cells are the ones in the bottoms of the grooves and the darker ones are the cells on the top plane of the coupon. The groove on the right is 40μm and the groove on the left is 30μm. Flow is from Right to Left.

Figure 15.

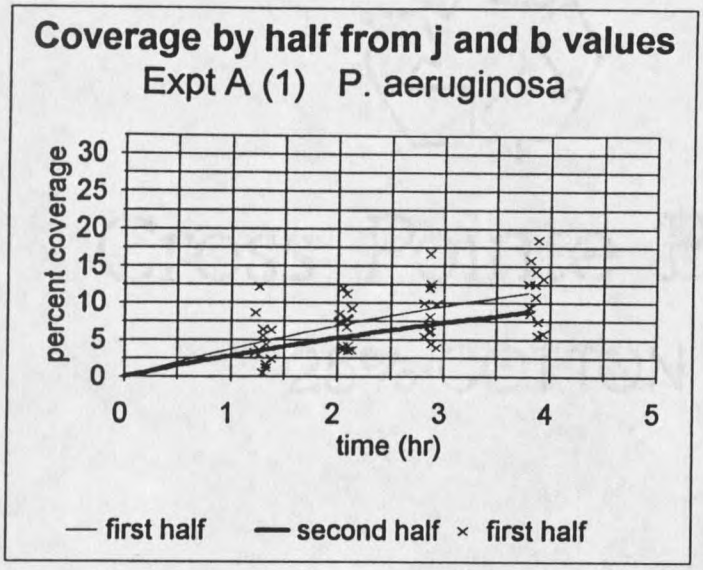

Figure 16.